# Observations and Mechanisms of a Simple Stochastic Dynamical Model

# Capturing El Niño Diversity

Nan Chen\*

- Department of Mathematics and Center for Atmosphere Ocean Science, Courant Institute of
- Mathematical Sciences, New York University, New York, NY, USA.
  - Andrew J. Majda
- 7 Department of Mathematics and Center for Atmosphere Ocean Science, Courant Institute of
- 8 Mathematical Sciences, New York University, New York, NY, USA,
- <sup>9</sup> Center for Prototype Climate Modeling, New York University Abu Dhabi, Saadiyat Island, Abu
- Dhabi, UAE.
- Sulian Thual
- Department of Mathematics and Center for Atmosphere Ocean Science, Courant Institute of
- Mathematical Sciences, New York University, New York, NY, USA.
- \*Corresponding author address: Nan Chen, Department of Mathematics and Center for Atmo-
- sphere Ocean Science, Courant Institute of Mathematical Sciences, New York University, 251
- Mercer Street, New York, NY 10012, USA.
- E-mail: chennan@cims.nyu.edu

# **ABSTRACT**

The El Niño-Southern Oscillation (ENSO) has significant impact on global climate and seasonal prediction. Recently, a simple modeling framework was developed that automatically captures the ENSO diversity, where statedependent stochastic wind bursts and nonlinear advection of sea surface temperature are coupled to a simple ocean-atmosphere model that is otherwise deterministic, linear and stable. In this article, the coupled model is compared with observations using reanalysis data during the last 34 years, where the observed non-Gaussian statistics and the overall mechanisms of ENSO are both captured by the model. Then the formation mechanisms of different types of El Niño based on the model are systematically studied. First, ocean Rossby waves induced by mean easterly trade wind anomalies facilitate the heat content buildup, which together with the reflected ocean Kelvin waves and the nonlinear advection create the central Pacific (CP) El Niño. Secondly, two formation mechanisms are revealed for the traditional El Niño, including the super El Niño. The first mechanism indicates an optimal wind structure with easterly wind bursts (EWBs) leading westerly wind bursts (WWBs) before the event peak, where the EWBs build up heat content that is transported eastward by the WWBs. The second mechanism links the two types of El Niño, where the CP El Niño prior to a traditional El Niño is responsible for the heat content buildup of the latter. This article also highlights the mechanisms of La Niña formation and El Niño breaking down as well as the importance of the nonlinear advection and boundary reflections.

### 1. Introduction

The El Niño-Southern Oscillation (ENSO) is the most prominent interannual climate variability on earth with large ecological and societal impacts. It consists of a cycle of anomalously warm El 42 Niño conditions and cold La Niña conditions with considerable irregularity in amplitude, duration, temporal evolution and spatial structure. The well-known traditional El Niño (or eastern Pacific (EP) El Niño) involves anomalous warm sea surface temperature (SST) in the equatorial eastern Pacific ocean, where its atmospheric response is the eastward shift of the anomalous Walker circulation with strong convection occurring near the west coast of America (Clarke 2008). In recent 47 decades, a different type of El Niño has been frequently observed, which is called the central Pacific (CP) El Niño (Lee and McPhaden 2010; Kao and Yu 2009; Ashok et al. 2007b; Kug et al. 2009; Larkin and Harrison 2005; Guilyardi 2006). The CP El Niño is characterized by warm SST anomalies confined to the central Pacific, flanked by colder waters to both east and west. Such zonal SST gradients result in an anomalous two-cell Walker circulation over the tropical Pacific, with strong convection located in the central Pacific (Kug et al. 2009). In addition to the distinct 53 climate patterns in the equatorial Pacific region, different types of El Niño and La Niña also have different teleconnections that affect the global climate and seasonal prediction (Ashok et al. 2007b; Weng et al. 2009; Capotondi et al. 2015). 56 The significant impact of ENSO requires a comprehensive understanding of the underlying for-57 mation mechanisms of different types El Niño as well as the development of dynamical models 58 that reproduce the ENSO diversity. However, most of the current climate models have biases in 59 simulating the ENSO diversity. Some general circulation models (GCMs) are able to reproduce only one single type of El Niño (Ham and Kug 2012; Kug et al. 2012; Ault et al. 2013; Capotondi 61 et al. 2015). Other climate models, despite their ability to reproduce the observed diversity of

- ENSO to some extent, typically overestimate the amplitude of the ENSO interannual variability and misrepresent the simulated frequency and duration of the El Niño events (Wittenberg 2009;
- Kug et al. 2010). In addition, these climate models are too complicated to be employed for under-
- standing the fundamental mechanisms of ENSO diversity.
- Recently, a simple modeling framework was developed that automatically captures the statistical
- diversity of ENSO (Thual et al. 2016; Chen and Majda 2016a,b). This simple modeling framework
- is physically consistent and amenable to detailed analysis, which facilitates the understanding of
- the formation mechanisms of ENSO diversity.
- In this simple modeling framework, the starting model involves a coupled ocean-atmosphere 71 model that is deterministic, linear and stable (Kleeman 2008; Kleeman and Moore 1997; Moore and Kleeman 1999). Then systematic strategies are developed for incorporating several major 73 causes of the ENSO diversity into the coupled system. First, a stochastic parameterization of the 74 wind bursts including both westerly and easterly winds is coupled to the simple ocean-atmosphere system, where the amplitude of the wind bursts depends on the strength of SST in the western Pacific warm pool through a Markov jump stochastic process. Such a coupled model is fundamentally different from the Cane-Zebiak (Zebiak and Cane 1987) and other nonlinear models (Jin 1997; Timmermann et al. 2003), for which the internal instability rather than the external wind bursts maintains the ENSO cycle. It is shown that (Thual et al. 2016) in addition to recovering traditional moderate El Niño and super El Niño as well as La Niña events, the coupled model is able to capture key features of the observational record in the eastern Pacific. Secondly, a simple nonlinear zonal advection with no ad-hoc parameterization of the background SST gradient is introduced that creates a coupled nonlinear advective mode of SST. In addition, due to the recent multidecadal strengthening of the easterly trade wind (England et al. 2014; Sohn et al. 2013; Merrifield and Maltrud 2011), a mean easterly trade wind anomaly is incorporated into the stochastic

parameterization of the wind activity. The combined effect of the nonlinear zonal advection, the
enhanced mean easterly trade wind anomaly and the effective stochastic noise facilitates the intermittent occurrence of the CP El Niño (Chen and Majda 2016a). Then, a three-state Markov jump
stochastic process is developed to drive the stochastic wind bursts. It emphasizes the distinct properties of the wind activity at different ENSO phases and describes the state-dependent transition
mechanisms in a simple and effective fashion. This simple stochastic switching process allows the
coupled model to simulate different types of ENSO events with realistic features (Chen and Majda
2016a,b).

In this article, the formation mechanisms of ENSO diversity based on this simple coupled mod-95 el are systematically studied and are compared with observational record using reanalysis data during the last 34 years. To begin with, the statistics in the observational data associated with 97 different variabilities are presented. It is shown that both the non-Gaussian statistical features and the overall ENSO formation mechanisms of the coupled model are highly consistent with nature. Then the formation mechanisms of different types of El Niño events based on the coupled model are explained with detailed analysis and concrete examples, where the significant roles of the un-101 derlying ocean Kelvin and Rossby waves as well as the wind burst activities are highlighted. First, 102 deterministic nonlinear advective modes are utilized to understand the formation mechanism of 103 the CP El Niño (Chen and Majda 2016a). It is shown that the mean easterly trade wind anomalies 104 are essential in triggering ocean Rossby waves that not only facilitate the heat content buildup 105 in the western Pacific but induce weak ocean Kelvin waves due to the imperfect reflection at the western Pacific boundary as well. Such consecutive Kelvin waves with weak amplitudes together 107 with the nonlinear advection are crucial in transporting the anomalous warm SST to the central 108 Pacific and maintaining the climate patterns there. By incorporating effective random wind bursts noise into the coupled system, more realistic features of CP El Niño events are reproduced. Sec-

ondly, two distinct mechanisms are revealed by the coupled model in the formation of traditional El Niño and super El Niño events. In addition to the bursts of westerly winds preceding the event 112 peak that drive anomalous warm SST to the eastern Pacific (Harrison and Vecchi 1997; Vecchi 113 and Harrison 2000; Tziperman and Yu 2007; Hendon et al. 2007), a series of strong easterly wind bursts (EWBs) (Hu and Fedorov 2016) are observed prior to those westerly wind bursts (WWBs) that contribute to the buildup of the heat content in the western Pacific. Such EWBs-WWBs wind 116 structure provides the first formation mechanism of a traditional El Niño event. The second formation mechanism links the CP El Niño and traditional El Niño. Since the heat content has already been transported to the central Pacific region during a CP event (Kug et al. 2009), a single WWB 119 right after the CP event is sufficient to push the anomalous warm water to the eastern Pacific and creates a traditional El Niño event. Distinct from the first mechanism, no pronounced EWB is 121 involved in this second formation mechanism. Next, according to the lagged correlations, La Niña 122 is shown to be the discharge phase following its preceding traditional El Niño and no significant 123 wind burst activity is observed at La Niña phases.

In addition to the formation of different ENSO events, the mechanism of El Niño breaking down, 125 such as the one observed in year 2014 (Hu and Fedorov 2016), is also explained. Furthermore, 126 examples show that strong wind bursts are necessary but not sufficient conditions for triggering 127 El Niño events (Fedorov et al. 2015; Hu et al. 2014; Roulston and Neelin 2000; Levine and Jin 128 2010). Finally, the deficiencies in various simplified versions of the coupled model highlight the 129 important roles of both the nonlinear advection and the eastern Pacific boundary reflections in the coupled model. The former is crucial in preventing the anomalous warm water being transported to 131 the eastern Pacific at CP El Niño phases while the latter is essential in obtaining realistic durations 132 of the traditional El Niño and particularly the super El Niño.

The remainder of this article is as follows. The coupled model is presented in Section 2, along 134 with a description of the processing of observational data. Section 3 shows the statistical features 135 and the overall ENSO formation mechanism of the coupled model, as compared with the obser-136 vations. The formation mechanisms of different types of El Niño and La Niña, in light of both 137 conditional statistics and case studies, are demonstrated in Section 4. In the same section, the underlying reasons for El Niño breaking down and some strong wind bursts not triggering any 139 El Niño are also revealed. The crucial roles of both the nonlinear advection and the reflection 140 boundary condition in the eastern Pacific are emphasized in Section 5. Summary conclusions are included in Section 6. 142

### 2. Model and Observational Data

a. Coupled ENSO Model

The ENSO model consists of a non-dissipative atmosphere coupled to a simple shallow-water ocean and SST budget in the interannual time scale (Thual et al. 2016; Chen and Majda 2016a,b):

Atmosphere model:

$$-yv - \partial_x \theta = 0,$$

$$yu - \partial_y \theta = 0,$$

$$-(\partial_x u + \partial_y v) = E_q/(1 - \overline{Q}),$$
(1)

148 Ocean model:

$$\partial_{\tau}U - c_1YV + c_1\partial_xH = c_1\tau_x,$$

$$YU + \partial_YH = 0,$$

$$\partial_{\tau}H + c_1(\partial_xU + \partial_YV) = 0,$$
(2)

SST model:

$$\partial_{\tau}T + \mu \partial_{x}(UT) = -c_{1}\zeta E_{q} + c_{1}\eta H, \tag{3}$$

150 with

$$E_q = \alpha_q T$$
, and  $\tau_x = \gamma(u + u_p)$ . (4)

In (1)–(4), x is zonal direction and  $\tau$  is interannual time, while y and Y are meridional direction 151 in the atmosphere and ocean, respectively. The u, v are zonal and meridional winds,  $\theta$  is potential 152 temperature, U, V, are zonal and meridional currents, H is thermocline depth, T is SST,  $E_q$  is 153 latent heating, and  $\tau_x$  is zonal wind stress, where  $u_p$  represents the wind bursts (see hereafter). All variables are anomalies from an equilibrium state, and are non-dimensional. The coefficient  $c_1$ 155 is a non-dimensional ratio of time scales, which is of order O(1). The term  $u_p$  in (4) describes 156 stochastic wind burst activity. The atmosphere extends over the entire equatorial belt  $0 \le x \le L_A$ with periodic boundary conditions, while the Pacific ocean extends over  $0 \le x \le L_0$  with reflection 158 boundary conditions for the ocean model and zero normal derivative at the boundaries for the SST 159 model. The parameter values of the coupled model are shown in Appendix A, and are the same as those in (Chen and Majda 2016a,b). 161

The above model retains a few essential processes that model the ENSO dynamics in a simple fashion. Latent heating  $E_q$ , proportional to SST, is depleted from the ocean and forces an atmospheric circulation. The resulting zonal wind stress  $\tau_x$  in return forces an ocean circulation that imposes feedback on the SST through thermocline depth anomalies H. This thermocline feedback  $\eta$  is more significant in the eastern Pacific, as shown in Figure 1.

The coupled model introduces unique theoretical elements such as a non-dissipative atmosphere consistent with the skeleton model for the Madden-Julian oscillation (MJO) (Majda and Stechmann 2009, 2011), valid here on the interannual timescale and suitable to describe the dynamics

of the Walker circulation (Majda and Klein 2003; Stechmann and Ogrosky 2014; Stechmann and Majda 2015). In addition, the meridional axis *y* and *Y* are different in the atmosphere and ocean as they each scale to a suitable Rossby radius. This allows for a systematic meridional decomposition of the system into the well-known parabolic cylinder functions (Majda 2003), which keeps the system low-dimensional (Thual et al. 2013) and will be discussed hereafter.

The coupled system (1)–(4) without the nonlinear zonal advection in (3) has been systematically studied in (Thual et al. 2016). It succeeds in recovering the traditional El Niño with occasional super El Niño as well as capturing the observed ENSO statistics in the eastern Pacific. Note that if the stochastic wind burst  $u_p$  is further removed, the resulting coupled system is linear, deterministic and stable (Kleeman 2008; Kleeman and Moore 1997; Moore and Kleeman 1999). Such a coupled model is fundamentally different from the Cane-Zebiak (Zebiak and Cane 1987) and other nonlinear models (Jin 1997; Timmermann et al. 2003) where the internal instability rather than the external wind bursts plays the role of maintaining the ENSO cycles.

The observational significance of the zonal advection has been shown for the CP El Niño (Kug 183 et al. 2009; Su et al. 2014). Different from the previous works (Jin and An 1999; Dewitte et al. 184 2013) where the advection is mostly linear and requires ad hoc parameterization of the background 185 SST gradient, a simple nonlinear advection is adopted in (3) that contributes significantly to the SST tendency. Such nonlinear advection provides the mechanism of transporting anomalous warm 187 water to the central Pacific region by the westward anomalous ocean zonal current. Importantly, 188 when stochasticity is included in the wind activity  $u_D$ , this nonlinear zonal advection involves the contribution from both mean and fluctuation, the latter of which is usually ignored in the previous 190 works. The combined effect of this nonlinear advection, a mean easterly trade wind anomaly and 191 effective stochastic noise was shown to facilitate the intermittent occurrence of the CP El Niño with realistic features (Chen and Majda 2016a).

### 194 1) MERIDIONAL TRUNCATION

For the purpose of solving and understanding the coupled system and retaining the key dynamical features, a simple meridional truncation is applied to the coupled model (1)–(3) (Thual et al. 2013, 2016).

Different parabolic cylinder functions are utilized in the ocean and atmosphere due to the d-198 ifference in their deformation radii. The zeroth-order atmospheric parabolic cylinder function has a Gaussian profile that is centered at the equator and reads  $\phi_0(y) = (\pi)^{-1/4} \exp(-y^2/2)$ , 200 and the second-order one which will be utilized as the reconstruction of solutions reads  $\phi_2=$ 201  $(4\pi)^{-1/4}(2y^2-1)\exp(-y^2/2)$ . The oceanic parabolic cylinder functions  $\psi_m(Y)$  are identical to 202 the expressions of the atmospheric ones except that they depend on the Y axis. In the atmo-203 sphere we assume a truncation of moisture, wave activity and external sources to the zeroth-order 204 parabolic cylinder function  $\phi_0$ . This is known to excite only the Kelvin and first Rossby atmospheric equatorial waves, of amplitude  $K_A$  and  $R_A$  (Majda and Stechmann 2009, 2011). In the 206 ocean (Clarke 2008), we assume a truncation of zonal wind stress forcing to  $\psi_0$ ,  $\tau_x = \tau_x \psi_0$ . This 207 is known to excite only the Kelvin and first Rossby oceanic equatorial waves, of amplitude  $K_O$  and  $R_O$ . Similarly, for the SST model we assume a truncation  $\psi_0$ ,  $T = T \psi_0$ . With these truncations, 209 the coupled ENSO model (1)–(3) becomes: 210

Atmosphere model:

$$\partial_{x}K_{A} = \chi_{A}(E_{q} - \langle E_{q} \rangle)(2 - 2\bar{Q})^{-1},$$

$$-\partial_{x}R_{A}/3 = \chi_{A}(E_{q} - \langle E_{q} \rangle)(3 - 3\bar{Q})^{-1},$$
(5)

Ocean model:

$$\partial_{\tau} K_O + c_1 \partial_x K_O = \chi_O c_1 \tau_x / 2,$$

$$\partial_{\tau} R_O - (c_1 / 3) \partial_x R_O = -\chi_O c_1 \tau_x / 3,$$
(6)

SST model:

$$\partial_{\tau}T + \mu \partial_{x} ((K_{O} - R_{O})T) = -c_{1} \zeta E_{q} + c_{1} \eta H, \tag{7}$$

where  $\chi_A$  and  $\chi_O$  are the projection coefficients from ocean to atmosphere and from atmosphere to ocean, respectively, because of the different extents in their meridional bases. Due to the absence of dissipation in the atmosphere, the solvability condition requires a zero equatorial zonal mean of latent heating forcing  $\langle E_q \rangle$  (Majda and Klein 2003; Stechmann and Ogrosky 2014). Note that when meridional truncation is implemented, a projection coefficient  $\chi \approx 0.65$  appears in front of the nonlinear term (Majda and Stechmann 2011), which is absorbed into the nonlinear advection coefficient  $\mu$  for the notation simplicity.

Periodic boundary conditions are adopted for the atmosphere model (5). Reflection boundary conditions are adopted for the ocean model (6),

$$K_O(0,t) = r_W R_O(0,t), \qquad R_O(L_O,t) = r_E K_O(L_O,t),$$
 (8)

where  $r_W = 0.5$  representing partial loss of energy in the west Pacific boundary across Indonesian and Philippine and  $r_E = 0.5$  representing partial loss of energy due to the north-south propagation of the coast Kelvin waves along the eastern Pacific boundary. For the SST model, no normal derivative at the boundary of T is adopted, i.e. dT/dx = 0.

Now instead of solving the original system (1)–(3), we solve the system with meridional truncation (5)–(7). The physical variables can be easily reconstructed in the following way.

$$u = (K_A - R_A)\phi_0 + (R_A/\sqrt{2})\phi_2,$$

$$\theta = -(K_A + R_A)\phi_0 - (R_A/\sqrt{2})\phi_2,$$

$$v = (4\partial_x R_A - \bar{H}A - S^{\theta})(3\sqrt{2})^{-1}\phi_1,$$

$$U = (K_O - R_O)\psi_0 + (R_O/\sqrt{2})\psi_2,$$

$$H = (K_O + R_O)\psi_0 + (R_O/\sqrt{2})\psi_2.$$
(9)

For the convenience of demonstration, all the variables shown below are at equator. See (Majda and Stechmann 2011; Thual et al. 2016; Chen and Majda 2016a,b) for more details.

## 2) STOCHASTIC WIND BURST PROCESS

Stochastic parameterization of the wind activity is added to the model that represents several important ENSO triggers such as the WWBs (Harrison and Vecchi 1997; Vecchi and Harrison 2000; Tziperman and Yu 2007), the EWBs (Hu and Fedorov 2016), as well as the convective envelope of the MJO (Hendon et al. 2007; Puy et al. 2016). It also includes the recent multidecadal strengthening of the easterly trade wind anomaly. The wind bursts  $u_p$  reads:

$$u_p = a_p(\tau)s_p(x)\phi_0(y), \tag{10}$$

with amplitude  $a_p(\tau)$  and fixed zonal spatial structure  $s_p(x)$  shown in Figure 1. Here,  $\phi_0(y)$  equals to the first parabolic cylinder function of the atmosphere. Both the wind burst perturbations (Tziperman and Yu 2007) and the strengthening of the trade wind anomaly (England et al. 2014; Sohn et al. 2013) are localized over the western equatorial Pacific according to the observations and for simplicity they share the same zonal extent.

The evolution of wind burst amplitude  $a_p$  reads:

242

$$\frac{da_p}{d\tau} = -d_p(a_p - \hat{a}_p(T_W)) + \sigma_p(T_W)\dot{W}(\tau), \tag{11}$$

where  $d_p$  is dissipation and  $\dot{W}(\tau)$  is a white noise source, representing the intermittent nature of the wind bursts at interannual timescale. The amplitude of the wind burst noise source  $\sigma_p$  depends on  $T_W$  (See Eq. (12)), which is the average of SST anomalies in the western half of the equatorial Pacific ( $0 \le x \le L_O/2$ ). Note that this state-dependent wind amplitude is fundamentally different from those in previous works (Jin et al. 2007; Levine and Jin 2015, 2010) that rely on the eastern Pacific SST. The term  $\hat{a}_p < 0$  represents the mean strengthening of the easterly trade

wind anomaly. Corresponding to  $\hat{a}_p < 0$ , the direct response of the surface wind associated with the Walker circulation at the equatorial Pacific band is shown in Panel (c) of Figure 1, which is similar to the observed intensification of the Walker circulation in recent decades (England et al. 2014; Sohn et al. 2013).

# 253 3) A THREE-STATE MARKOV JUMP STOCHASTIC PROCESS

Due to the fact that the ENSO diversity is associated with the wind activity with distinct features 254 (Thual et al. 2016; Chen and Majda 2016a), a three-state Markov jump stochastic process (Gar-255 diner et al. 1985; Lawler 2006; Majda and Harlim 2012) is adopted to describe the wind activity. 256 Here, State 2 primarily corresponds to the traditional El Niño and State 1 to the CP El Niño while 257 State 0 represents discharge and quiescent phases. The following criteria are utilized to determine 258 the parameters in (11) in each state. First, strong wind bursts play an important role in triggering 259 the traditional El Niño (Vecchi and Harrison 2000; Tziperman and Yu 2007; Hendon et al. 2007), 260 which suggests a large noise amplitude  $\sigma_p$  in State 2. Secondly, the observational fact that an 261 enhanced easterly trade wind accompanies with the CP El Niño since 1990s indicates a negative 262 (easterly) mean  $\hat{a}_p$  in State 1. To obtain the CP El Niño, the amplitude of  $\hat{a}_p$  and the stochastic noise must be balanced (Chen and Majda 2016a). This implies a moderate noise amplitude in 264 State 1, which also agrees with observations (Chen et al. 2015). Finally, only weak wind activity 265 is allowed in the quiescent state and the discharge phase with La Niña (State 0). Thus, the three states are given by 267

State 2: 
$$\sigma_{p2} = 3.75$$
,  $d_{p2} = 5.1$ ,  $\hat{a}_{p2} = -0.25$ ,  
State 1:  $\sigma_{p1} = 1.2$ ,  $d_{p1} = 5.1$ ,  $\hat{a}_{p1} = -0.25$ , (12)  
State 0:  $\sigma_{p0} = 0.5$ ,  $d_{p0} = 5.1$ ,  $\hat{a}_{p0} = 0$ ,

respectively, where  $d_p = 5.1$  represents a relaxation time around 6.67 days. Note that the same mean easterly trade wind anomaly as in State 1 is adopted in State 2 due to the fact that both the traditional and the CP El Niño occurred during the last 25 years. Since the amplitude of the stochastic noise dominates the mean easterly wind in State 2, this mean state actually has little impact on simulating the traditional El Niño events. On the other hand, to guarantee no El Niño event occurring in the quiescent phase, no mean trade wind anomaly is imposed in State 0. With such choice of the parameters, both the amplitude and the timescale of the wind burst activity are similar to nature.

The local transition probability from State i to State j with  $i \neq j$  for small  $\Delta \tau$  is defined as follows

$$P(\sigma_p(\tau + \Delta \tau) = \sigma_{pi} | \sigma_p(\tau) = \sigma_{pi}) = v_{ij} \Delta \tau + o(\Delta \tau), \tag{13}$$

278 and the probability of staying in State i is given by

$$P(\sigma_p(\tau + \Delta \tau) = \sigma_{pi} | \sigma_p(\tau) = \sigma_{pi}) = 1 - \sum_{j \neq i} v_{ij} \Delta \tau + o(\Delta \tau).$$
 (14)

Importantly, the transition rates  $v_{ij}$  (with  $i \neq j$ ) depend on  $T_W$ , implying the state-dependence of the wind bursts (Levine et al. 2016; Lopez and Kirtman 2013; Lopez et al. 2013). A transition  $v_{ij}$  (with i < j) from a less active to a more active state is more likely when  $T_W \geq 0$  and vice versa. This allows for example a rapid shutdown of wind burst activity followed by extreme El Niño events, as in nature.

The transition rates are chosen in accordance with the observational record. A higher transition probability from State 2 to State 0 is adopted compared with that to State 1, representing the situation that the traditional El Niño is usually followed by the La Niña rather than the CP El Niño (e.g., years 1963, 1965, 1972, 1982, 1987 and 1998.) Likewise, starting from the quiescent phase, the model has a preference towards the occurrence of the CP El Niño rather than the eastern Pacific

super El Niño, as observed in years 1968, 1990 and 2001. See Appendix B for details. It is shown in (Chen and Majda 2016b) that the model statistics is robust with respect to the perturbation of the parameters, which indicates that a crude estimation of the transition rates is sufficient for obtaining the ENSO diversity with realistic features.

The parameterization of the wind activity in (10)–(14) emphasizes the distinct properties of the wind activity at different ENSO phases and describes effective state-dependent transitions in a simple and effective fashion. It is different from those adopted in previous works that involve many complicated and detailed structures, such as the central location and peak time of each wind burst event (Gebbie and Tziperman 2009; Gebbie et al. 2007; Tziperman and Yu 2007) and the separation of the linear and nonlinear parts of the wind activity (Levine and Jin 2015).

# 299 b. Definitions of Different El Niño Events in the Coupled Model

In order to compare the model simulations with the observational record, we make use of the three well-known Nino SST indices: Nino 3 (150W-90W), Nino 3.4 (170W-120W) and Nino 4 (160E-150W).

The definitions of the traditional El Niño and the La Niña are quite simple: with anomalous SST above 0.5K and below -0.5K in Nino 3 region. On the other hand, the identification of a CP El Niño event requires the combination of different Nino indices and an uniform definition is still under debate (Ashok et al. 2007a; Trenberth and Stepaniak 2001; Kug et al. 2009; Yeh et al. 2009; Ren and Jin 2011).

Here, simple criteria are proposed to distinguish different El Niño events are proposed in light
of the distinct roles of each of the three states in the wind activity model. Specifically, situating
in State 1 is one of the necessary conditions for identifying the CP El Niño. Other conditions for
recognizing a CP El Niño event are Nino 4>Nino 3> 0. The reason to pick up Nino 3> 0 here

is to exclude the La Niña-like events and such positive value of the averaged SST over Nino 3 region isn't incompatible with the CP El Niño feature that cooling occurs near the eastern Pacific 313 boundary. Note that replacing Nino 4 by Nino 3.4 for identifying the CP El Niño doesn't lead 314 to qualitative difference in any of the statistical features shown below thanks to the constraint of situating in State 1. On the other hand, although strong wind bursts (State 2) trigger the traditional El Niño, the decaying phase of each traditional El Niño event from anomalously warm SST back to 317 the normal condition corresponds to State 0. In addition, the ENSO discharge phase with La Niña 318 also typically lies in State 0 with occasional occurrences in State 2. Thus, traditional El Niño and La Niña requires locating in either State 0 or 2. Other conditions for traditional El Niño are Nino 320 3>0.5 and Nino 3>Nino 3.4, where the latter serves to exclude CP-like events that occasionally occur in State 2, and those for La Niña are Nino 3<-0.5. These criteria are summarized in Table 322 1. 323

### 324 c. Observational Data

In this work, observational data is utilized to assess the realism of the model solutions. The 325 following three observational datasets are utilized: 1) daily zonal winds at 850hPa from the 326 NCEP/NCAR reanalysis (Kalnay et al. 1996) (http://www.esrl.noaa.gov/psd/), 2) daily sea surface temperatures from the OISST reanalysis (Reynolds et al. 2007) (https://www. 328 ncdc.noaa.gov/oisst), and 3) monthly thermocline depth from the NCEP/GODAS reanalysis 329 (Behringer et al. 1998) (http://www.esrl.noaa.gov/psd/). Thermocline depth is computed 330 from potential temperature as the depth of the 20C isotherm. All datasets are averaged meridion-331 ally within 5N-5S in the tropical Pacific (120E-80W) and cover the period from January 1982 to 332 September 2016.

From the data, we obtain fields of zonal winds  $u_{OBS}(x,t)$  in  $m.s^{-1}$ , sea surface temperature  $T_{OBS}(x,t)$  in K, and thermocline depth  $H_{OBS}(x,t)$  in m that depend only on zonal position x (deg lon) and time t (days). In addition, we define  $u_{OBS}^W(t)$  as the amplitude of zonal winds anomalies  $u_{OBS}$  in the western Pacific, computed from an average in the region 140E-180E. This average is roughly equivalent to a projection on the zonal wind burst structure  $s_p(x)$  of the ENSO model defined in Figure 1.

Each field is decomposed into climatology, interannual anomalies and intraseasonal anomalies.

For example, zonal winds is decomposed into:

$$u_{OBS}(x,t) = u_{SC}(x,t) + u_A(x,t) + u_{HF}(x,t)$$
(15)

where  $u_{SC}$  is climatology,  $u_A$  is interannual anomalies to the climatology, and  $u_{HF}$  is intraseasonal 342 anomalies. For this, a 90-days centered running mean is applied to  $u_{OBS}$  from which  $u_{HF}$  is 343 extracted as residual. The running mean signal is then decomposed into climatology  $u_{SC}$  and anomalies  $u_A$  using seasonal averages. A similar decomposition is utilized for  $T_{OBS}$ ,  $H_{OBS}$  and 345  $u_{OBS}^{W}$ . 346 The observed fields presented above are the potential surrogates for the variables in the simple ENSO model described in Section 2a. Observed zonal winds anomalies  $u_A + u_{HF}$ , sea surface 348 temperature anomalies  $T_A + T_{HF}$  and thermocline depth anomalies  $H_A + H_{HF}$  are direct surrogates 349 for  $u + u_p$ , T and H in the model, respectively. 350 In the comparison of the statistics below, the model variables are also decomposed into in-351 terannual and intraseasonal anomalies utilizing the same method as described above. The only 352 difference is that there is no seasonal cycle in the model.

# 3. Observations, Statistical Properties and Overall Mechanisms of ENSO

### 355 a. Observed ENSO Variabilities

The observed ENSO variabilities in the equatorial Pacific during the last 34 years are shown in Figure 2. The general circulation in the equatorial Pacific region consists of strong trade winds 357 in the central Pacific as well as strong zonal gradients of SST and thermocline depth (See Pan-358 el (d), (f) and (h)). Such a general circulation is destablized during El Nino events as positive SST anomalies develop in the central-eastern Pacific along with enhanced eastward zonal wind-360 s and strong thermocline depth anomalies (See Panel (c), (e), (g)). Particularly, the traditional 361 El Niño with maximum SST anomalies in the eastern Pacific is distinguished from the CP El Niño with maximum SST anomalies in the central Pacific. Major traditional El Niño events occur 363 in years 1982/1983, 1997/1998, 2006/2007 and 2015/2016 while prominent CP El Niño events 364 are observed in years 1987/1988, 1990/1991, 1992/1993, 1994/1995, 2002/2003, 2004/2005 and 2009/2010. Note that a traditional El Niño is usually followed by a La Nina with reverse condi-366 tions. In addition, Figure 2 shows the details of wind bursts activity according to the intraseasonal 367 zonal winds over the entire tropical Pacific  $(u_{HF})$  or averaged in the western Pacific  $(u_{HF}^{W})$ . Wind 368 burst activity is highly irregular and intermittent with both westerly and easterly wind bursts. 369 Figure 3 shows linear trends in time for the observed zonal winds, SST and thermocline depth 370 over the period 1982-2016. A displacement of the trade winds from the central-eastern to the central Pacific is clearly observed. Particularly, the decreased averaged value of the observed 372 zonal wind over the western Pacific indicates a multidecadal strengthening of the easterly trade 373 wind there (England et al. 2014; Sohn et al. 2013; Merrifield and Maltrud 2011). This justifies 374 imposing the mean easterly trade wind anomaly  $\hat{a}_p$  into the coupled model (11). On the other hand, both SST and thermocline depth show a gradual increase during the last 34 years.

# b. Statistical Properties of the Model and Observations

We start with exploring the statistical properties of both the coupled model and observations.

The statistics of the model is based on a 5000-year-long simulation. Figure 4 and 5 show the probability density functions (PDFs) for interannual anomalous SST, zonal winds and thermocline depth associated with the coupled model and observations, respectively.

First, consistent with observations, the PDFs of SST associated with the coupled model in Ni-382 no 4 and Nino 3 regions show negative and positive skewness, respectively. The presence of a 383 fat tail together with the positive skewness in Nino 3 indicates the extreme El Niño events in 384 the eastern Pacific (Burgers and Stephenson 1999). Note that, despite the correct skewed di-385 rection, the skewness of  $T_A$  of the model in Nino 3 region seems to be underestimated com-386 pared with that of the observations. Yet, the observations only contain a 34-year-long record 387 (1982-2016), which may not be sufficient to form unbiased statistics. In fact, the single super El Niño event during 1997-1998 accounts for a large portion of the skewness in Nino 3. 389 On the other hand, despite a slight overestimation, the variance in all the three Nino region-390 s associated with the model almost perfectly match those with observations. Particularly, the fact that the variance of SST in Nino 4 region being roughly half as much as that in the oth-392 er two regions is captured by the coupled model. Note that, as described in the previous work 393 (Thual et al. 2016; Chen and Majda 2016b), the parameters in the coupled model are calibrated within physically reasonable ranges to match the SST variances with those provided by NOAA 395 (https://www.ncdc.noaa.gov/teleconnections/enso/indicators/sst.php). The Nino 396 indices in different regions are all slightly larger than the observational values utilized here. The reason for this is that the climatology computed here is based on the whole 34-year period 1982-398 2016 while only the data before 2000 is utilized in NOAA's version. As shown in Figures 2 and 3, the SST has an increased trend especially after year 2000, which implies a larger amplitude of climatology and in turn a smaller variance in the SST anomalies of the observations.

Next, the zonal winds and thermocline depth are averaged over three different regions: the 402 western Pacific (140E-180), the central Pacific (180-140W) and the eastern Pacific (140E-100W). The PDFs of the observed zonal surface winds in the central and eastern Pacific are both positively skewed and fat-tailed. Such non-Gaussian features are successfully captured by the coupled model. 405 Although the associated variance from the model simulation as shown in Figure 4 seems to be 406 underestimated, decreasing of both the wind stress coefficient  $\gamma$  in the ocean model and the latent 407 heat feedback coefficient Q in the atmosphere model within a physically reasonable range serve to 408 enhance the variance of the winds while leaving other variabilities unaffected. On the other hand, 409 the variances of the observed thermocline depth in all the three regions are well captured by the coupled model. 411

In addition to the PDFs, the autocorrelation function of the total wind bursts anomalies  $a_{all}$  in-412 cluding both the interannual and the intraseasonal components is shown in Panel (a) of Figure 6 and that containing only the interannual wind bursts anomalies  $a_A$  resulting from the 90-day run-414 ning average is shown in Panel (b). A short memory of  $a_{all}$ , around 6 to 7 days, is revealed, which 415 is affirmed by the damping coefficient  $d_p$  in (12). On the other hand, the interannual anomalies of the wind bursts has a longer memory, around 2-3 months. Both values are consistent with obser-417 vations (Levine and Jin 2015; Tziperman and Yu 2007; Yu et al. 2003). Finally, Panel (c) in Figure 418 6 shows the power spectrum of the interannual SST anomalies averaged over the eastern Pacific  $(L_O/2 < x < L_O)$ . The peak is at the interannual band (3-7 years), as in the observations (Kleeman 420 2008). 421

All these findings indicate that the statistical features of the model are quite consistent with nature.

# 424 c. Overall Mechanism of ENSO formation

To understand the overall mechanism of ENSO formation, lagged correlation between Nino 3.4 425 SST index and different variabilities are shown in Figure 7 for the observations and in Figure 8 426 for the coupled model. The lagged correlations with SST  $T_A$ , thermocline  $H_A$ , zonal wind  $u_A$  and 427 the zonal wind averaged over the western Pacific  $u_A^W$  are all shown in both figures. Making use 428 of the advantage of the model that the wind bursts can be extracted from the overall zonal winds, 429 the lagged correlation with the overall wind bursts  $a_{all}$  and its interannual component  $a_A$  are also 430 shown in Figure 8. Note that except Panel (e) in Figure 8, all the variabilities utilized here are 431 the interannual with a 90-day running average as discussed in Section 2c. Here, focus is on the 432 overall formation mechanism that includes all events while the formation mechanisms conditioned 433 on different types of El Niño will be discussed in Section 4. 434

As shown in Figure 7, El Niño events are typically preceded by a buildup phase around 1 to 2 years prior to the event peak, during which SST and thermocline depth gradually enhance in the western Pacific. Then, during the trigger phase around 0.5 year prior to the event peak, strong westerly zonal surface winds, positive SST and thermocline depth anomalies all develop and propagate from the western to the central-eastern Pacific. Importantly, in addition to a strong positive correlation between Nino 3.4 index and the zonal wind averaged over the western Pacific  $u_A^W$  which is less than 1 year prior to it, a weak negative correlation is found at lag times about 1-3 years. All these features are captured by the coupled model with an exceptionally high skill.

Apparently, the positive correlation with  $u_A^W$  is mainly due to the reversal of anomalous Walker circulation at the onset of an El Niño event as well as the presence of WWBs that serve to trigger the El Niño. On the other hand, the appearance of the weak negative correlation with  $u_A^W$  remains ambiguous by simply looking at the observational data. Nevertheless, due to the advantage of

the model that the wind bursts can be completely extracted from the total atmosphere wind, the lagged correlations between the Nino 3.4 and the wind bursts are shown in Panel (e) and (f) of 448 Figure 8. These lagged correlations provide a significant evidence that the EWBs contribute to the 449 negative correlation in the total winds. In fact, such EWBs facilitate the buildup of heat content in the western Pacific, which is crucial in the formation of El Niño events. Details will be shown in 451 Section 4.

In Figure 8, the overall mechanism of ENSO formation was revealed and the results from the

coupled model are highly consistent with nature (Figure 7). Nevertheless, each type of El Niño

#### 4. Mechanisms for the Formations of Different Events and Case Studies

454

455

468

has its unique formation mechanism that is distinct from the overall behavior. Understanding 456 the difference in these formation mechanisms is of importance. However, within the 34-year short observational period, each type of El Niño events appear only a few times. Such a small 458 number of samples is not sufficient for arriving at any unbiased conclusions. On the other hand, 459 the simple coupled dynamical model, which has been shown to possess the statistical features that is qualitatively similar as nature, is able to provide simulations with much longer period, which 461 facilitates the understanding of the formation mechanisms of ENSO diversity within this simple 462 coupled model. Below, a 5000-year-long simulation from the coupled dynamical model is utilized for under-464 standing the formation mechanisms of different events. Here is the summary of what we present 465 below. The lagged correlations conditioned on traditional El Niño, La Niña and CP El Niño phases, respectively, are shown in Figure 9. Figure 10 illustrates the deterministic advective modes 467 from the coupled nonlinear model associated with the CP El Niño (Chen and Majda 2016a). Fig-

uring out the interactions between different waves and their link with physical variables in these

deterministic modes facilitates the understanding of more complicated stochastic model. Figure
11 shows properties of the waiting time between the occurrence of a CP El Niño event and its previous and adjacent traditional El Niño, which improves the understanding of the transition
mechanism between these two types of events. Finally, Figure 12–15 include case studies of the
formation and development of different El Niño events and are linked with the general discussions
of the statistical features. A description of each case study is summarized in Table 2.

Same as in the previous section, the statistical features shown in Figure 9 and in Panel (a)-(d) of Figure 11 are all computed based on the interannual variables (with subscript  $\cdot_A$ ). On the other hand, in order to see the structure of the wind bursts activity and the evolution of different types of waves, the raw output from the model that includes both interannual and intraseasonal components is shown in different case studies.

#### 481 a. CP El Niño

#### 482 1) STATISTICAL FEATURES

Row 3 in Figure 9 shows the conditional lagged correlations between the Nino 4 SST index and different fields conditioned on CP El Niño phases, where the criteria for identifying the CP El Nino phases was discussed in Section 2b. The Nino 4 SST index is utilized here due to the fact that CP El Niño is more related to the anomalous warm SST near dateline rather than the eastern Pacific.

First, different from the overall events (Figure 8) and the eastern Pacific El Niño/La Niña (Row 1-2 in Figure 9) in which significant correlations (|Corr| > 0.5) appear only at lag times less than 1 year, the Nino 4 SST index conditioned on CP El Nino phases has strong correlations with different fields even at 2- to 3-year lag times. This reveals the intrinsic difference between CP and traditional events that a CP El Niño episode can have a longer duration up to 4-5 years. Next, the

maximum correlation of Nino 4 index with both SST and thermocline appears in the central Pa-493 cific, as expected. This is consistent with the positive and negative correlations of the atmosphere 494 surface wind  $u_A$  in the western and eastern Pacific, respectively, which indicates the structure of the 495 anomalous Walker circulation that the surface winds converge in the central Pacific region. One noticeable feature for the CP El Niño is the flux divergence  $-\mu \partial_x (UT)$ . The lagged correlation 497 structure in Panel (e) illustrates the role of the flux divergence in warming and cooling the SST in 498 the central-western and central-eastern Pacific, respectively. Therefore, the flux divergence serves 499 to transport anomalous warm SST from the eastern Pacific to the central region that is crucial in the formation of CP El Niño. Finally, corresponding to the mean easterly trade wind anomaly at 501 the CP El Niño phases, a negative lagged correlation is found between the Nino 4 index and the wind bursts  $a_A$ .

### 504 2) DETERMINISTIC ADVECTION MODES

To see the development of waves and different physical variables in the formation of CP El Niño 505 events, we start with the deterministic nonlinear advection modes (Chen and Majda 2016b). Here, 506 the stochastic noise in (11) is removed and the wind activity  $a_p \equiv \hat{a}_p$  becomes a constant. Based 507 on different values of the nonlinear advection  $\mu$  and the amplitude of the easterly mean trade wind anomaly  $a_p$ , three dynamical regimes are found in Panel (a) of Figure 10. In regime I, the steady-509 state solution has constant values at each longitude. Particularly, with a suitably strong  $a_p$  and 510 even without the nonlinear advection, the anomalous warm SST is shifted to the central-eastern Pacific region. The corresponding anomalous ocean zonal current is westward and the anomalous 512 atmospheric surface winds converge in the central-eastern Pacific as well. On the other hand, 513 when both  $\mu$  and  $a_p$  are sufficiently large (Regime III), the steady-state solution shows regular

oscillation patterns with period around 1.6 years. Within each period, warm water is transported westward and the maximum of anomalous warm SST is at the central and central-eastern Pacific. 516 The most important dynamical regime (Regime II) is shown in Panel (c), which is directly as-517 sociated with the CP El Niño when random wind bursts are included. This dynamical regime requires a nonzero zonal advection and a suitably strong easterly trade wind anomaly  $a_p$ , such that 519 all of the fields becomes time-periodic, and the period is much longer than 2 years. Starting from 520 a nearly quiescent phase, the easterly mean trade wind anomaly triggers ocean Rossby waves that 521 propagate westward (t = 88). When these Rossby waves arrive at the western Pacific boundary, the reflection boundary condition induces ocean Kelvin waves that propagate eastward, where the 523 amplitude of the reflected Kelvin waves is weaker than the Rossby waves due to the energy loss at the boundary. The combined effect of these Rossby and Kelvin waves results in an increase 525 of the thermocline depth and SST anomalies in the western Pacific. As a direct response to the 526 latent heat, the atmosphere winds become stronger and the westerly and easterly surface winds 527 converge in the central Pacific region (t = 90). Then, due to the fact that atmosphere winds force ocean waves (See Eq. (6)), the westerly atmosphere winds in the western Pacific push the reflected 529 weak ocean Kelvin waves to the central Pacific, while the easterly winds in the eastern Pacific pre-530 vent these weak waves arriving at the eastern Pacific boundary. Meanwhile, these easterly winds 531 have the wind stress which develops ocean Rossby waves, with amplitudes that peak at the central 532 Pacific. Since thermocline depth is directly linked to the amplitude of ocean Kevlin and Rossby 533 waves (See Eq. (9)), an increase of the thermocline depth occurs in the central Pacific region, which leads to the build-up of anomalous warm SST. Note that due to the fact that ocean Ross-535 by waves have stronger amplitudes than ocean Kelvin waves, a westward anomalous ocean zonal 536 current appears in the central Pacific region (See Eq. (9)), which together with the profile of SST anomalous results in a westward transport of anomalous warm water via the nonlinear advection 538

of SST, and brings about the eastern Pacific cooling. These anomalous warm SST then stays and gradually develops in the central Pacific for a few years (t = 95). As the westward ocean zonal current and the atmosphere easterly winds in the central and eastern Pacific continue to strengthen, the anomalous warm SST is transported to the western pacific with a deeper thermocline there. Such strong heat content storage provides the condition of triggering a strong traditional El Niño (t = 108), followed by which is a discharge phase of La Niña that drives all the fields back to a nearly quiescent state.

### 46 3) CASE STUDIES

Now we go back to the full model with effective state-dependent stochastic noise in the wind activity (11)–(14). Case study (IV) in Figure 13 shows a period of 2.5-year CP El Niño from t = 413.5 to t = 416.

First, the interannual wind time series in Panel (f) clearly indicates a mean easterly trade wind 550 anomaly. Starting from t = 413, moderate and weak ocean Rossby waves are triggered continu-551 ously by this mean trade wind anomaly together with the effective stochastic wind bursts noise, 552 and heat content starts to accumulate in the western Pacific. Due to the imperfect reflection at the 553 western Pacific boundary  $r_W = 0.5$ , the reflected Kelvin waves have only weak amplitudes. Such weak Kelvin waves are able to transport heat content eastward and adjust the atmosphere zonal 555 wind structure (Compare t = 413 and 414 in Panel (a)). However, due to the sea-air interaction, the 556 easterly atmosphere zonal surface winds in the eastern surface Pacific also weaken these Kelvin 557 waves (See Eq. (6)). Eventually, a balance is established in the central Pacific region. On the 558 other hand, this atmosphere zonal wind structure also induces ocean Rossby waves that start from 559 the eastern Pacific and peak at the location where easterly and westerly surface winds converge (See Eq. (6)). Thus, according to the link between ocean waves and thermocline depth (9), the maximum of the heat content appears in the central Pacific and results in the CP El Niño.

Note that the reflected weak Kelvin waves created by the mean easterly trade anomaly are crucial in the formation of the CP El Niño. As will be seen in Section 4b, strong Kelvin waves induced by the WWBs are able to overcome the barriers from atmosphere easterly zonal winds and therefore transport the heat content and anomalous warm SST to the eastern Pacific and eventually change the atmosphere wind structure.

Budget analysis is illustrated in Figure 15. Panel (d) shows the flux divergence  $-\mu \partial_x (UT)$ , which at the CP El Niño phases serves to increase and decrease SST anomalies in the central-western and central-eastern Pacific, respectively. On the other hand, the combined effect of the damping  $-c_1\zeta E_q$  and thermocline feedback  $c_1\eta H$  as shown in Panel (e) indicates an opposite structure with an increased SST tendency in the eastern Pacific. Note that, even if the cooling  $-c_1\zeta E_q$  is excluded from the combined effect, the thermocline feedback still tends to warm the central-eastern Pacific (Panel (g)). In fact, as will be shown in Section 5, the thermocline feedback in the coupled model without the nonlinear zonal advection only warms the eastern Pacific and that model fails to reproduce CP El Niño .

# b. Traditional El Niño Including Super El Niño

## 1) Two Formation Mechanisms

Row 1 of Figure 9 shows the lagged correlation between Nino 3 SST index and different fields conditioned on the traditional El Niño phases. The lagged correlations up to 1-year lag times for all fields are quite similar to those of the overall events (Figure 8). Particularly, in addition to the positive correlation with the WWBs occurring a few months prior to the event peak, a significant negative correlation between Nino 3 SST and wind bursts is found around 1 year before the event

peak, which corresponds to the appearance of the EWBs. Such EWBs are crucial for inducing and accumulating heat content in the western Pacific that facilitates the following WWBs to trigger El
Niño. This provides the first formation mechanism of the traditional El Niño.

Formation mechanism 1: EWBs appear around 1 year before a traditional El Niño event, which induce the buildup of anomalous warm SST and heat content in the western Pacific. Such EWBs are followed by a series of WWBs occurring a few months prior to the event peak, which lead to the eastward propagation of the anomalous warm SST and heat content to the eastern Pacific and simultaneously alter the zonal circulation of the anomalous atmosphere winds.

In addition to the strong lagged correlation at a lag time around 1 year as discussed above,
Row 1 of Figure 9 also reveals moderate correlations between Nino 3 index and both SST and
thermocline in the central and western Pacific at time lag up to 3.5 years. Meanwhile, moderate
correlations with westerly and easterly zonal atmosphere winds in the western and eastern Pacific
are also noticeable. These lagged correlation structures resemble those in the CP El Niño phase.
In fact, a second formation mechanism of the traditional El Niño is linked to its previous CP El
Niño.

Formation mechanism 2: In the presence of a CP El Niño event, both the anomalous SST and
heat content have been transported to the central Pacific. Thus, instead of triggering heat content
in the western Pacific by a series of EWBs, a single strong WWBs right after a CP El Niño event
is sufficient to push the anomalous warm water and heat content from the central Pacific to the
eastern Pacific and forms the traditional El Niño. No significant EWBs is observed during this
process.

### 5 2) CASE STUDIES

Figure 12 shows two case studies that belong to formation mechanisms 1 and 2, respectively.

Case study (I) illustrates the formation mechanism 1, where a moderate traditional El Niño and 607 a super El Niño are shown. Both events are isolated traditional El Niño that are not led by CP El 608 Niño. Starting from t = 1236, a series of EWBs occur, which induces strong ocean Rossby waves 609 in the western Pacific. These ocean Rossby waves propagate westward and form Kelvin waves after they reflect at the western Pacific boundary. During this process, heat content represented 611 by thermocline depth is accumulated in the western Pacific, due to the positive amplitudes of both 612 Kelvin and Rossby waves (See Eq. (9)). Then around t = 1237 a series of WWBs arise and bring about significant ocean Kelvin waves, which transport strong heat content and SST to the eastern Pacific and form a super El Niño. Finally, the Kelvin waves reflect at the eastern Pacific 615 boundary and induce Rossby waves. These reflected Rossby waves are crucial in obtaining the realistic duration of the El Niño event. In fact, Case study (SII) in Section 5 shows that in the absence of the reflected Rossby waves the durations of the simulated traditional El Niño events are 618 much shorter than those in nature. Similarly, the moderate traditional El Niño around t = 1243 is formed by the EWBs-WWBs mechanism. Note that the accumulated heat content in the western Pacific induced by the ocean Rossby waves is one of the most crucial factors that determine the 621 strength of the El Niño in the eastern Pacific. Other factors affecting the El Niño strength include 622 the amplitudes of both the WWBs and EWBs as well as the profile of their interannual profile. In 623 Figure 15, budget analysis shows that thermocline feedback plays the most important role in the 624 formation of a traditional El Niño event, which is different from the CP El Niño where the flux 625 divergence is the dominant factor. 627

Case study (II) in Figure 12 describes the formation of a super El Niño in the eastern Pacific based on mechanism 2. First, a series of CP El Niño is developed (t = 365-368), accompanied by which is a mean easterly trade wind anomaly. Different from Case study (I) that EWBs trigger heat content in the western Pacific that prepares the formation of a traditional El Niño, the heat

content in Case study (II) has already been transported to the central Pacific region due to the CP El Niño (Kug et al. 2009). Then, with the presence of a series of WWBs (t = 368), both the heat and anomalous warm SST are transported from the central Pacific to the eastern Pacific and a super El Niño is formed. Clearly, the fact that no obvious EWB appears prior to the WWBs in Case study (II) distinguishes the two mechanisms.

In Figure 13, two more case studies are included. Case study (III) is similar to Case study (II).

But the heat content in the central Pacific during CP El Niño phase in Case study (III) is weaker
than that in (II) and therefore the subsequent WWBs cause a moderate traditional El Niño rather
than a super El Niño. In Case Study (IV), there is a short quiescent phase between the CP and the
traditional El Niño events. Therefore, the two events should be treated as separate events despite
that the overall profiles look similar to those in (III), and thus the EWBs-WWBs structure is needed
in Case (IV) to form a traditional El Niño event.

3) WAITING TIME BETWEEN A CP EL NIÑO EVENT AND ITS PREVIOUS ADJACENT TRADI TIONAL EL NIÑO

As was seen in the previous subsection, a traditional El Niño event is likely to follow a series of

CP El Niño events, which is partly due to the prescribed high transition rate from State 1 to State

2 based on the observational evidence. Yet, understanding the reverse situation, i.e., the waiting

time between a CP El Niño and its previous adjacent traditional El Niño, is equally crucial in

interpreting the mutual effect between these two types of El Niño.

The distribution of such waiting time can be obtained by searching both types of events from the long-term model simulations. Recall that the definition of a CP event was provided in Table 1. For the traditional El Niño events, in addition to the standard definition with Nino 3 > 0.5, different threshold values of Nino 3 are adopted, which allows us to include from all traditional El

Niño events to only super El Niño events. Note that when the threshold value becomes large, more moderate and weak traditional El Niño events will appear between a CP El Niño and its previous adjacent super El Niño.

In Panel (a) of Figure 11, the standard definition of the traditional El Niño is adopted, i.e., 657 Nino 3 > 0.5, which leads to a bimodal distribution of the waiting time. The major mode peaks 658 around 3.5 years while the peak of the minor mode is around 1 years. Such bimodality implies 659 two different scenarios. In the first scenario, a traditional El Niño is followed by a La Niña, and 660 then after 1-2 years quiescent period, a CP El Niño appears. Examples are shown in Panel (e). In fact, the observed episodes during 1987-1990 and 1998-2002 both belong to the first situation. In 662 the second scenario, a CP El Niño occurs right after a traditional El Niño, where an example is shown in Panel (f). Clearly, this second situation occurs less frequently than the first one in the model simulation. It is also observed only in years 1977-1978 during the last 50 years (Chen et al. 665 2015). Particularly, with the enhancing of the threshold of the Nino 3 index for the traditional El 666 Niño, the minor mode disappears and the resulting distribution of waiting time is unimodal (Panel (d)), which implies that the second situation happens only when the traditional El Niño has weak 668 amplitude. In fact, a La Niña usually follows a moderate or strong traditional El Niño in order to 669 discharge the heat content. 670

### 671 c. La Niña

The formation mechanism of La Niña is relatively simple. Lagged correlations in Row 2 of
Figure 9 show that both the SST anomalies and the heat content propagate from western Pacific to
eastern Pacific. A negative correlation between Nino 3 index and SST anomalies at a lag time of
2 years in Row 2 is consistent with that at 2 years lead time in Row 1 that is conditioned on the
traditional El Niño phases. Both indicate that La Nina serves as the discharge phase of El Niño.

- This argument is further validated by the lagged correlation between Nino 3 index and wind bursts  $a_A$ , where WWBs occur 1.5 prior to the La Nina event peak and trigger the previous recharge phases that corresponds to a traditional El Niño event.
- In Case study (I)-(IV), a traditional El Niño is always followed by a La Niña, where only little
  wind bursts are found during all the La Niña phases. In addition, the anomalous Walker circulation
  at La Niña phases is nearly opposite to that at traditional El Niño phases.

# 683 d. An El Niño breaking down by EWBs

As was seen in Case study (I) that a specific wind burst structure, where EWBs lead WWBs, triggers a traditional El Niño. Yet, different wind burst structures are observed in nature. Actually, a reverse wind structure, namely EWBs following WWBs, occurred during year 2014, where a strong EWB stalled the development of a potential traditional El Niño that was triggered by its previous WWBs (Hu and Fedorov 2016). Case (V) in Figure 14 exhibits an example with such wind burst structure and provides a simple mechanism for EWBs' impeding the development of a traditional El Niño.

In Case (V), a series of WWBs around t = 480.3 induces ocean Kelvin waves, which propagate eastward and bring anomalous warm SST to the eastern Pacific. These WWBs also cool the western Pacific and lead to a negative amplitude of Rossby waves in the western Pacific. Due to such anomalous cool water, the subsequent EWBs around t = 480.8 are unable to build up heat content in the western Pacific. Instead, they induce ocean Kelvin waves with negative amplitude. These negative Kelvin waves propagate eastwards and suppress the positive Rossby waves reflected by the previous positive Kelvin waves. Therefore, the eastern Pacific becomes cooler and the development of the traditional El Niño is stalled.

# e. Strong Wind Bursts with No/Weak El Niño

714

Traditional El Niño events are typically triggered by wind bursts activities (Harrison and Vecchi 700 1997; Vecchi and Harrison 2000; Tziperman and Yu 2007; Hendon et al. 2007). However, there are 701 many examples that wind burst activity builds up without triggering any El Niño event, implying 702 that wind burst activity in the model is a necessary but non-sufficient condition to the El Niño 703 development (Hu et al. 2014; Fedorov et al. 2015; Roulston and Neelin 2000; Levine and Jin 2010). 705 Case studies (VI) in Figure 14 illustrate two wind structures, in which strong wind bursts lead to 706 no or very weak El Niño. In (VI.a), both WWBs and EWBs appear with large amplitudes and the 707 interannual component is even not close to zero. However, the total wind profile switches between 708 these two types of wind bursts with a high frequency. In (VI.b), the interannual wind bursts stay 709 near zero and the intraseasonal wind bursts resemble white noise. The common feature in the two scenarios is that no enough heat content is able to build up in the western Pacific and no warm 711 water is able to accumulate in the eastern Pacific. Therefore, wind bursts with long durations and 712

# 5. Various Simplifications of the Coupled Model and their Dynamical Deficiencies

resulting from the wind bursts is the essence that facilitates the El Niño formation.

To understand the role of several important components in the coupled ENSO model (1)–(3),
different simplified versions of the coupled model are studied in this section.

strong amplitudes are not sufficient to trigger El Niño events. The buildup of the heat content

The first simplification involves dropping the nonlinear ocean zonal advection ( $\mu = 0$ ) in the SST equation (3), where a case study is shown in Figure 16. This simplified model retains the traditional El Niño and La Niña (t = 275-278). In fact, as was shown in the previous work (Thual et al. 2016), traditional El Niño was successfully simulated by the coupled model even in the

absence of the nonlinear advection. However, without the nonlinear zonal advection, the coupled model has difficulties in reproducing the CP El Niño with realistic features. The major issue is that 723 the location of the anomalous warm SST at State 1 shifts from the central Pacific to the central-724 eastern or eastern Pacific (t = 268-269 and t = 278-281). In fact, budget analysis in Figure 15 already indicates the key role of the nonlinear advection, without which the combined effect of the 726 thermocline feedback and cooling only leads to the anomalous warm SST in the eastern Pacific. 727 In addition, the deterministic modes in Figure 10 (Regime I) implies that the strengthening of the 728 trade wind anomaly itself is insufficient to transport the anomalous warm SST to the central Pacific region. It is the combined effect of the strengthening of the trade wind and the nonlinear zonal 730 advection that develops and maintains the CP El Niño. 731

Another important element in the coupled model is the ocean reflection condition at the eastern 732 Pacific boundary  $r_E$ , which hasn't been emphasized yet. In fact, this ocean boundary reflection is 733 essential for obtaining the realistic features of the traditional El Niño and particularly the super El 734 Niño. To see the role of  $r_E$ , a reduced model with  $r_E = 0$  is utilized, where a case study is shown in Figure 17. Despite that the reduced model is able to reproduce the CP El Niño as in nature 736 (t = 256-260 and t = 266-267), the duration of the traditional El Niño (t = 261, 264.5 and 269.5)737 is much shorter than the observed ones (years 1982, 1998 and 2016 in Figure 2). Particularly, the duration of the super El Niño is only about 3 months (t = 264.5), which is much shorter than 739 the observations. Note that the thermocline depth, which is the dominant contributor to the SST 740 tendency at the traditional El Niño phase, is given by the linear superposition of ocean Kelvin and ocean Rossby waves (See (7) and (9)). Since the wave speed of the Rossby wave is only 1/3 742 as much as that of the Kelvin wave, the Rossby wave plays an important role in maintaining the 743 anomalous warm SST at the traditional El Niño phase. However, with  $r_E = 0$ , there is no reflected ocean Rossby waves, which results in the short duration of the traditional El Niño events. 745

### **6. Discussion and Conclusions**

Understanding the formation mechanisms of ENSO diversity has significant impact on global climate and seasonal prediction. Recently, a simple modeling framework has been developed that automatically captures the statistical properties and key features of ENSO diversity. This sim-749 ple modeling framework is physically consistent and amenable to detailed analysis. The starting 750 model in this framework is a simple ocean-atmosphere model that is deterministic, linear and sta-751 ble. Then several key features are incorporated into the coupled system to capture several major 752 causes of the ENSO diversity. These key features are state-dependent stochastic wind bursts and 753 nonlinear advection of SST which allow effective transitions between different ENSO states. 754 In this article, the formation mechanisms of ENSO diversity based on this simple coupled model 755 are systematically studied. In Section 3, the statistics in the observational data associated with dif-756 ferent variabilities are illustrated. The non-Gaussian statistical properties in nature are all successfully captured by the coupled model and the overall ENSO formation mechanism of the coupled 758 model are highly consistent with that of the real observations. In Section 4, the formation mech-759 anisms of different types of El Niño and La Niña based in the coupled model are discussed. It is shown in the model with only the deterministic nonlinear advective modes that the mean easterly 761 trade wind anomaly is essential in triggering ocean Rossby waves that not only facilitate the heat 762 content buildup in the western Pacific but also induce reflected ocean Kelvin waves with weak amplitude. The reflected ocean Kelvin waves, combined with the nonlinear advection, are espe-764 cially crucial in maintaining the climate patterns associated with the CP El Niño (Chen and Majda 765 2016a). Incorporating effective random wind bursts into the nonlinear advective modes results in more realistic features of the CP El Niño. Two mechanisms are revealed for the formation of 767 traditional El Niño events. The first mechanism involves an EWBs-WWBs structure of the wind

activity that corresponds to the buildup of the heat content in the western Pacific and the transport of the anomalous warm water to the eastern Pacific, respectively. The second mechanism links the 770 CP El Niño and traditional El Niño, where a single WWB occurring right after a CP El Niño is 771 sufficient to push the anomalous warm water to the eastern Pacific. On the other hand, La Niña is 772 proved to be the discharge phase of traditional El Niño. In addition to the ENSO formation, the underlying reasons for some strong wind bursts not triggering any El Niño and specific EWBs' 774 stalling the development a traditional El Niño event are also explained in Section 4. In Section 5, 775 several simplified versions of the coupled model are utilized to highlight the crucial roles of both the nonlinear advection and the boundary reflections in the eastern Pacific that contribute to the 777 realistic features of CP and traditional El Niño, respectively. 778

As mentioned at the end of Section 2, seasonal cycle, which allows most of the El Niño events

peak at the end of the years, hasn't been incorporated into the coupled model. Therefore, including

seasonal cycle into the simple modeling framework will be one of the future works. Another future

work is the El Niño prediction, which requires developing an effective data assimilation scheme

for the coupled model as initialization and designing practical prediction algorithms.

Acknowledgments. The research of A.J.M. is partially supported by the Office of Naval Research
 Grant ONR MURI N00014-16-1-2161 and the New York University Abu Dhabi Research Institute.
 N.C. and S.T. are supported as postdoctoral fellows through A.J.M's ONR MURI Grant.

87 APPENDIX A

### Choices of parameter values

Two tables are included below. Table A1 summarizes the variables in the coupled model and lists the associated units and the typical unit values. Table A2 shows the nondimensional values of the parameters that are utilized in the meridional truncated model (5)–(7).

APPENDIX B

793

798

799

800

801

802

803

806

807

#### Details of the transition rates in the three-state Markov jump stochastic process

Recall in (11)–(14), a three-state Markov jump stochastic process is adopted for describing the wind activity. The criteria of transitions between different states were briefly mentioned there and the details are listed as follows. These transition rates are determined in accordance with the observational facts in Figure 2 and reference (Chen et al. 2015).

• The transition rates from State 2 to State 1 and from State 2 to State 0 are given by respectively

$$v_{21} = \frac{1}{10} \cdot \frac{1 - \tanh(2T_W)}{4},\tag{B1}$$

$$v_{20} = \frac{9}{10} \cdot \frac{1 - \tanh(2T_W)}{4}.$$
 (B2)

Starting from State 2, the probability of switching to State 0 is much higher than that to State 1. This comes from the fact that a traditional El Niño is usually followed by a La Niña rather than a CP El Niño (e.g., year 1963, 1965, 1972, 1982 and 1998). Typically, the La Niña event has a weaker amplitude and a longer duration compared with the preceding El Niño. This actually corresponds to a discharge phase of the ENSO cycle with no external wind bursts (State 0).

• The transition rates from State 1 to State 0 and from State 1 to State 2 are given by respectively

$$v_{10} = \frac{1 - \tanh(2T_W)}{12},\tag{B3}$$

$$v_{12} = \frac{1 + \tanh(2T_W)}{40},\tag{B4}$$

Although the denominator of  $v_{10}$  is smaller than that of  $v_{12}$ , quite a few CP El Niño events are associated with a slight positive  $T_W$  in the model, which means the transition rate  $v_{12}$  is not necessarily smaller than  $v_{10}$ . In fact, with the transition rates given by (B3)–(B4), the results show in the main article that more events are transited from state 1 to 2 than from state 1 to 0. This is consistent with the observations (e.g., year 1981 and 1995), implying that the CP El Niño is more likely to be followed by the classical El Niño than the quiescent phase.

• The transition rates from State 0 to State 1 and State 2 are given by

$$v_{01} = \frac{2}{3} \cdot \frac{1 + \tanh(2T_W)}{7},\tag{B5}$$

$$v_{02} = \frac{1}{3} \cdot \frac{1 + \tanh(2T_W)}{7}.$$
 (B6)

Again, the transition rates to State 1 and 2 are different. This is due to the fact that after a quiescent period or discharge La Niña phase, more events are prone to becomes CP El Niño as a intermediate transition instead of directly forming another traditional El Niño (e.g., year 1969, 1977, 1990 and 2002).

Note that in (B1)–(B6), the transition rate  $v_{ij}$  from a more active state to a less active state (with i>j) is always proportional to  $1-\tanh(2T_W)$  while that from a less active state to a more active state (with i< j) is always proportional to  $1+\tanh(2T_W)$ . These are consistent with the fact stated in the main article that a transition from a less active to a more active state is more likely when  $T_W \geq 0$  and vice versa.

#### 25 References

Ashok, K., S. K. Behera, S. A. Rao, H. Weng, and T. Yamagata, 2007a: El Niño Modoki and its possible teleconnection. *Journal of Geophysical Research: Oceans*, **112** (**C11**).

- Ashok, K., S. K. Behera, S. A. Rao, H. Weng, and T. Yamagata, 2007b: El Nino Modoki and its 828 possible teleconnections. J. Geophys. Res, 112. 829
- Ault, T., C. Deser, M. Newman, and J. Emile-Geay, 2013: Characterizing decadal to centennial 830 variability in the equatorial Pacific during the last millennium. Geophysical Research Letters,
- **40** (**13**), 3450–3456. 832

- Behringer, D. W., M. Ji, and A. Leetmaa, 1998: An improved coupled model for ENSO prediction and implications for ocean initialization. Part I: The ocean data assimilation system. *Monthly* 834 Weather Review, **126** (4), 1013–1021.
- Burgers, G., and D. B. Stephenson, 1999: The "normality" of El Niño. Geophys. Res. Lett, 26 (8), 1027–1039. 837
- Capotondi, A., and Coauthors, 2015: Understanding ENSO diversity. Bulletin of the American *Meteorological Society*, **96** (**6**), 921–938.
- Chen, D., and Coauthors, 2015: Strong influence of westerly wind bursts on El Niño diversity. 840 *Nature Geoscience*, **8** (**5**), 339–345. 841
- Chen, N., and A. J. Majda, 2016a: Simple dynamical models capturing the key features of the 842 central Pacific El Niño. Proceedings of the National Academy of Sciences, 113 (42), 11732-843 11737.
- Chen, N., and A. J. Majda, 2016b: Simple stochastic dynamical models capturing the statistical 845 diversity of El Niño Southern Oscillation. Proceedings of the National Academy of Sciences, submitted.
- Clarke, A. J., 2008: An Introduction to the Dynamics of El Nino & the Southern Oscillation. 848 Academic press.

- Dewitte, B., S.-W. Yeh, and S. Thual, 2013: Reinterpreting the thermocline feedback in the
- western-central equatorial Pacific and its relationship with the ENSO modulation. Climate dy-
- namics, **41** (**3-4**), 819–830.
- England, M. H., and Coauthors, 2014: Recent intensification of wind-driven circulation in the
- Pacific and the ongoing warming hiatus. *Nature Climate Change*, **4** (3), 222–227.
- Fedorov, A. V., S. Hu, M. Lengaigne, and E. Guilyardi, 2015: The impact of westerly wind bursts
- and ocean initial state on the development, and diversity of El Niño events. Climate Dynamics,
- **44 (5-6)**, 1381–1401.
- <sup>858</sup> Gardiner, C. W., and Coauthors, 1985: *Handbook of Stochastic Methods*, Vol. 3. Springer Berlin.
- 6859 Gebbie, G., I. Eisenman, A. Wittenberg, and E. Tziperman, 2007: Modulation of westerly wind
- bursts by sea surface temperature: A semistochastic feedback for ENSO. Journal of the Atmo-
- spheric Sciences, **64** (**9**), 3281–3295.
- <sup>862</sup> Gebbie, G., and E. Tziperman, 2009: Predictability of SST-modulated westerly wind bursts. *Jour-*
- nal of Climate, **22** (**14**), 3894–3909.
- Guilyardi, E., 2006: El Nino-mean state-seasonal cycle interactions in a multi-model ensemble.
- 865 Climate Dynamics, **26** (**4**), 329–348.
- Ham, Y.-G., and J.-S. Kug, 2012: How well do current climate models simulate two types of El
- Nino? Climate dynamics, **39** (1-2), 383–398.
- Harrison, D., and G. A. Vecchi, 1997: Westerly wind events in the Tropical Pacific, 1986-95\*.
- *Journal of climate*, **10** (**12**), 3131–3156.
- Hendon, H. H., M. C. Wheeler, and C. Zhang, 2007: Seasonal dependence of the MJO-ENSO
- relationship. *Journal of Climate*, **20** (3), 531–543.

- Hu, S., and A. V. Fedorov, 2016: Exceptionally strong easterly wind burst stalling El Niño of 2014. *Proceedings of the National Academy of Sciences*, **113** (**8**), 2005–2010.
- Hu, S., A. V. Fedorov, M. Lengaigne, and E. Guilyardi, 2014: The impact of westerly wind
- bursts on the diversity and predictability of El Niño events: an ocean energetics perspective.
- *Geophysical Research Letters*, **41** (**13**), 4654–4663.
- Jin, F.-F., 1997: An equatorial ocean recharge paradigm for ENSO. Part I: Conceptual model.
- Journal of the Atmospheric Sciences, **54** (**7**), 811–829.
- Jin, F.-F., and S.-I. An, 1999: Thermocline and zonal advective feedbacks within the equatorial
- ocean recharge oscillator model for ENSO. *Geophysical research letters*, **26** (**19**), 2989–2992.
- Jin, F.-F., L. Lin, A. Timmermann, and J. Zhao, 2007: Ensemble-mean dynamics of the EN-
- SOecharge oscillator under state-dependent stochastic forcing. *Geophysical research letters*,
- 883 **34 (3)**.
- Kalnay, E., and Coauthors, 1996: The NCEP/NCAR 40-year reanalysis project. Bulletin of the
- American meteorological Society, **77** (3), 437–471.
- 886 Kao, H.-Y., and J.-Y. Yu, 2009: Contrasting eastern-Pacific and central-Pacific types of ENSO.
- <sup>887</sup> *Journal of Climate*, **22** (**3**), 615–632.
- Kleeman, R., 2008: Stochastic theories for the irregularity of ENSO. *Philosophical Transac*-
- tions of the Royal Society of London A: Mathematical, Physical and Engineering Sciences,
- **366 (1875)**, 2509–2524.
- Kleeman, R., and A. M. Moore, 1997: A theory for the limitation of ENSO predictability due to
- stochastic atmospheric transients. *Journal of the atmospheric sciences*, **54** (6), 753–767.

- Kug, J.-S., J. Choi, S.-I. An, F.-F. Jin, and A. T. Wittenberg, 2010: Warm pool and cold tongue
- El Niño events as simulated by the GFDL 2.1 coupled GCM. *Journal of Climate*, **23** (5), 1226–
- 895 1239.
- 896 Kug, J.-S., Y.-G. Ham, J.-Y. Lee, and F.-F. Jin, 2012: Improved simulation of two types of El Niño
- in CMIP5 models. *Environmental Research Letters*, **7** (**3**), 034 002.
- Kug, J.-S., F.-F. Jin, and S.-I. An, 2009: Two types of El Niño events: cold tongue El Niño and
- warm pool El Niño. *Journal of Climate*, **22 (6)**, 1499–1515.
- Larkin, N. K., and D. Harrison, 2005: On the definition of El Niño and associated seasonal average
- US weather anomalies. *Geophysical Research Letters*, **32** (13).
- Lawler, G. F., 2006: Introduction to Stochastic Processes. CRC Press.
- Lee, T., and M. J. McPhaden, 2010: Increasing intensity of El Niño in the central-equatorial
- Pacific. *Geophysical Research Letters*, **37** (**14**).
- Levine, A., F. F. Jin, and M. J. McPhaden, 2016: Extreme Noise-extreme El Niño: How state-
- dependent noise forcing creates el niño-la niña asymmetry. *Journal of Climate*.
- Levine, A. F., and F.-F. Jin, 2010: Noise-induced instability in the ENSO recharge oscillator.
- Journal of the Atmospheric Sciences, 67 (2), 529–542.
- Levine, A. F., and F. F. Jin, 2015: A simple approach to quantifying the noise–ENSO interac-
- tion. Part I: deducing the state-dependency of the windstress forcing using monthly mean data.
- 911 Climate Dynamics, 1–18.
- Lopez, H., and B. P. Kirtman, 2013: Westerly wind bursts and the diversity of ENSO in CCSM3
- and CCSM4. Geophysical Research Letters, 40 (17), 4722–4727.

- Lopez, H., B. P. Kirtman, E. Tziperman, and G. Gebbie, 2013: Impact of interactive westerly wind bursts on CCSM3. *Dynamics of Atmospheres and Oceans*, **59**, 24–51.
- Majda, A., 2003: *Introduction to PDEs and Waves for the Atmosphere and Ocean*, Vol. 9. American Mathematical Soc.
- Majda, A. J., and J. Harlim, 2012: Filtering Complex Turbulent Systems. Cambridge University
   Press.
- Majda, A. J., and R. Klein, 2003: Systematic multiscale models for the tropics. *Journal of the Atmospheric Sciences*, **60** (2), 393–408.
- Majda, A. J., and S. N. Stechmann, 2009: The skeleton of tropical intraseasonal oscillations. *Proceedings of the National Academy of Sciences*, **106 (21)**, 8417–8422.
- Majda, A. J., and S. N. Stechmann, 2011: Nonlinear dynamics and regional variations in the MJO skeleton. *Journal of the Atmospheric Sciences*, **68** (**12**), 3053–3071.
- Merrifield, M. A., and M. E. Maltrud, 2011: Regional sea level trends due to a Pacific trade wind intensification. *Geophysical Research Letters*, **38 (21)**.
- Moore, A. M., and R. Kleeman, 1999: Stochastic forcing of ENSO by the intraseasonal oscillation. *Journal of Climate*, **12** (**5**), 1199–1220.
- Puy, M., J. Vialard, M. Lengaigne, and E. Guilyardi, 2016: Modulation of equatorial Pacific westerly/easterly wind events by the Madden–Julian oscillation and convectively-coupled Rossby waves. *Climate Dynamics*, **46** (**7-8**), 2155–2178.
- Ren, H.-L., and F.-F. Jin, 2011: Niño indices for two types of ENSO. *Geophysical Research*Letters, **38 (4)**.

- Reynolds, R. W., T. M. Smith, C. Liu, D. B. Chelton, K. S. Casey, and M. G. Schlax, 2007:
- Daily high-resolution-blended analyses for sea surface temperature. *Journal of Climate*, **20** (22),
- <sub>937</sub> 5473–5496.
- Roulston, M. S., and J. D. Neelin, 2000: The response of an ENSO model to climate noise, weather noise and intraseasonal forcing. *Geophysical research letters*, **27** (**22**), 3723–3726.
- Sohn, B., S.-W. Yeh, J. Schmetz, and H.-J. Song, 2013: Observational evidences of Walker circu-
- lation change over the last 30 years contrasting with GCM results. *Climate Dynamics*, **40** (7-8),
- 942 1721–1732.
- Stechmann, S. N., and A. J. Majda, 2015: Identifying the skeleton of the Madden–Julian oscillation in observational data. *Monthly Weather Review*, **143** (1), 395–416.
- Stechmann, S. N., and H. R. Ogrosky, 2014: The Walker circulation, diabatic heating, and outgo ing longwave radiation. *Geophysical Research Letters*, 41 (24), 9097–9105.
- Su, J., T. Li, and R. Zhang, 2014: The initiation and developing mechanisms of central Pacific El
  Niños. *Journal of Climate*, **27** (**12**), 4473–4485.
- Thual, S., A. J. Majda, N. Chen, and S. N. Stechmann, 2016: Simple stochastic model for El Niño with westerly wind bursts. *Proceedings of the National Academy of Sciences*, 201612002.
- Thual, S., O. Thual, and B. Dewitte, 2013: Absolute or convective instability in the equatorial Pacific and implications for ENSO. *Quarterly Journal of the Royal Meteorological Society*, 139 (672), 600–606.
- Timmermann, A., F.-F. Jin, and J. Abshagen, 2003: A nonlinear theory for El Niño bursting.

  Journal of the atmospheric sciences, **60** (**1**), 152–165.

- Trenberth, K. E., and D. P. Stepaniak, 2001: Indices of El Niño evolution. *Journal of Climate*, 14 (8), 1697–1701.
- Tziperman, E., and L. Yu, 2007: Quantifying the dependence of westerly wind bursts on the largescale tropical Pacific SST. *Journal of climate*, **20** (**12**), 2760–2768.
- Vecchi, G. A., and D. Harrison, 2000: Tropical Pacific sea surface temperature anomalies, El Nino, and equatorial westerly wind events. *Journal of climate*, **13** (**11**), 1814–1830.
- Weng, H., S. K. Behera, and T. Yamagata, 2009: Anomalous winter climate conditions in the
  Pacific rim during recent El Niño Modoki and El Niño events. *Climate Dynamics*, **32** (**5**), 663–674.
- Wittenberg, A. T., 2009: Are historical records sufficient to constrain ENSO simulations? *Geo-*physical Research Letters, **36** (**12**).
- Yeh, S.-W., J.-S. Kug, B. Dewitte, M.-H. Kwon, B. P. Kirtman, and F.-F. Jin, 2009: El Niño in a changing climate. *Nature*, **461** (**7263**), 511–514.
- Yu, L., R. A. Weller, and W. T. Liu, 2003: Case analysis of a role of ENSO in regulating the generation of westerly wind bursts in the western equatorial pacific. *Journal of Geophysical Research: Oceans*, **108** (C4).
- <sup>972</sup> Zebiak, S. E., and M. A. Cane, 1987: A model El Niño-Southern oscillation. *Monthly Weather*<sup>973</sup> *Review*, **115** (**10**), 2262–2278.

974	LIST	<b>OF</b>	<b>TABLES</b>	
-----	------	-----------	---------------	--

975	Table A1.	Definitions of model variables and units in the meridional truncated model	47
976	Table A2.	Nondimensional values of the parameters	48
977	Table 1.	Criteria of defining different ENSO events.	49
978	Table 2.	Summary of case studies	50

Table A1. Definitions of model variables and units in the meridional truncated model.

Variable	unit	unit value
x zonal axis	$[y]/\delta$	15000km
y meridional axis atmosphere	$\sqrt{c_A/eta}$	1500km
Y meridional axis ocean	$\sqrt{c_O/eta}$	330km
t time axis intraseasonal	$1/\delta\sqrt{c_Aoldsymbol{eta}}$	3.3 days
au time axis interannual	[t]/arepsilon	33 days
u zonal wind speed anomalies	$\delta c_A$	$5 ms^{-1}$
v meridional wind speed anomalies	$\delta[u]$	$0.5  ms^{-1}$
$\theta$ potential temperature anomalies	15δ	1.5 <i>K</i>
q low-level moisture anomalies	[ heta]	1.5 <i>K</i>
a envelope of synoptic convective activity	1	
$\overline{H}a$ convective heating/drying	[ heta]/[t]	$0.45  K.day^{-1}$
$E_q$ latent heating anomalies	[ heta]/[t]	$0.45  K.day^{-1}$
T sea surface temperature anomalies	[ heta]	1.5 <i>K</i>
U zonal current speed anomalies	$c_O \delta_O$	$0.25  ms^{-1}$
V zonal current speed anomalies	$\delta \sqrt{c}[U]$	$0.56cms^{-1}$
H thermocline depth anomalies	$H_O\delta_O$	20.8 <i>m</i>
$ au_x$ zonal wind stress anomalies	$\delta\sqrt{\beta/c_A}H_O\rho_Oc_O^2\delta_O$	$0.00879 N.m^{-2}$
$\tau_y$ meridional wind stress anomalies	$[ au_x]$	$0.00879 N.m^{-2}$

Table A2. Nondimensional values of the parameters.

Parameter	description	Nondimensional values
с	ratio of ocean and atmosphere phase speed	0.05
ε	Froude number	0.1
$c_1$	ratio of $c/arepsilon$	0.5
XA	Meridional projection coefficient from ocean to atmosphere	0.31
χο	Meridional projection coefficient from atmosphere to ocean	1.38
$L_A$	Equatorial belt length	8/3
$L_O$	Equatorial Pacific length	1.16
γ	wind stress coefficient	6.529
$r_W$	Western boundary reflection coefficient in ocean	0.5
$r_E$	Eastern boundary reflection coefficient in ocean	0.5
ζ	Latent heating exchange coefficient	8.5
$\alpha_q$	Latent heating factor	0.3782
Q	mean vertical moisture gradient	0.9
μ	nonlinear zonal advection coefficient	0.08
$d_p$	dissipation coefficient in the wind burst model	3.4

TABLE 1. Criteria of defining different ENSO events.

	Condition 1	Condition 2	Condition 3
Traditional El Niño	State 0 or 2	Nino 3 > 0.5	Nino 3 > Nino 3.4
La Niña	State 0 or 2	Nino 3 < -0.5	
CP El Niño	State 1	Nino 4 > Nino 3 > 0	

TABLE 2. Summary of case studies.

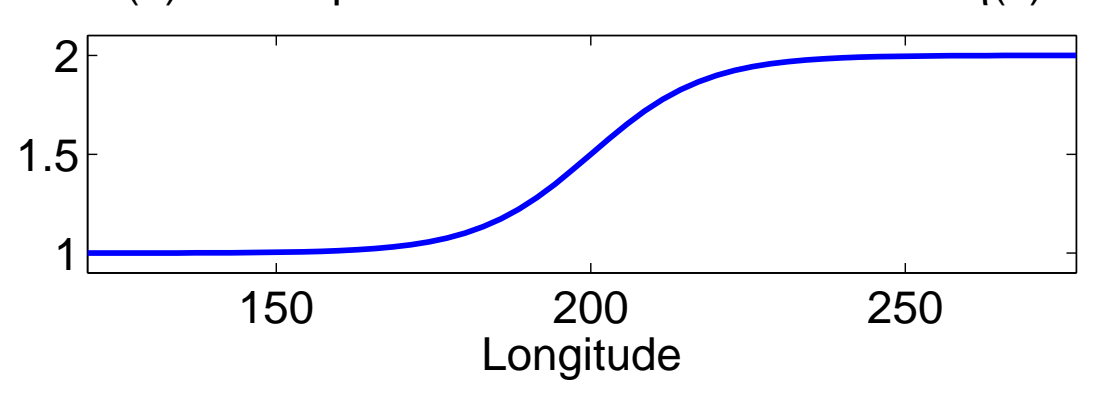
Case	Figure #.	Event type
(I)	12	An isolated moderate traditional El Niño and an isolated super El Niño
(II)	12	A series CP El Niño followed directly by a super El Niño
(III)	13	A series CP El Niño followed directly by a moderate traditional El Niño
(IV)	13	A traditional El Niño following a series of CP El Niño with a short quiescent phase in between
(V)	14	An EWB stalling the development of a traditional El Niño
(VI)	14	Strong wind bursts but no/weak El Niño
(SI)	16	Model without zonal advection: Failure in simulating CP El Niño
(SII)	17	Model no reflection in the eastern Pacific boundary: Failure in simulating traditional El Niño with realistic features

### 979 LIST OF FIGURES

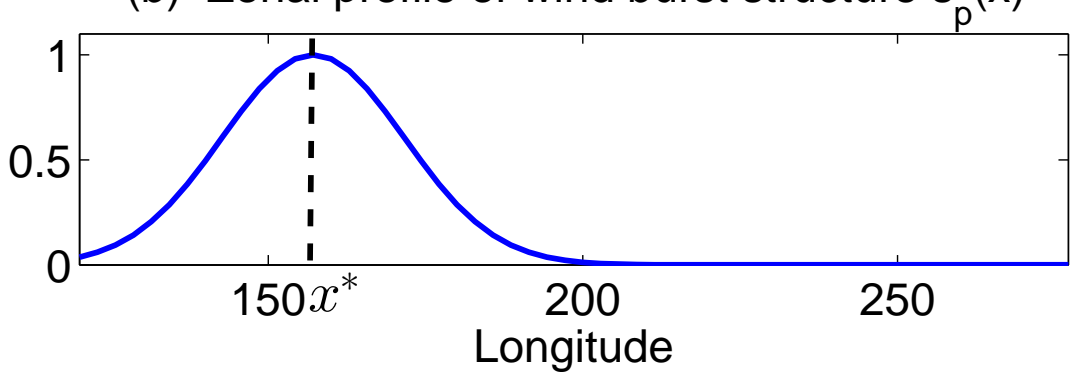
980 981 982	Fig. 1.	(a) Zonal profile of thermocline feedback $\eta(x)$ . (b) Zonal profile of wind burst structure $s_p(x)$ in the western Pacific. (c) Surface wind response directly to the mean easterly trade wind anomaly $\hat{a}_p$ , i.e. $\hat{a}_p \cdot s_p(x) \cdot \phi_0(y)$	53
983 984 985 986 987 988 989	Fig. 2.	Observed ENSO variability. (a) Zonal winds averaged over the western Pacific (140E-180), with a superposition of interannual $u_A^W$ (black) and intraseasonal $u_{HF}^W$ (blue for $u_{HF}^W < 0$ , red for $u_{HF}^W > 0$ ) anomalies. (b) Hovmoller of strong intraseasonal zonal winds $u_{HF}$ (blue for $u_{HF} \le -5 \ m.s^{-1}$ , red for $u_{HF} \ge 5 \ m.s^{-1}$ ). (c) Hovmoller of zonal winds anomalies $u_A$ . (d) Hovmoller of zonal winds anomalies and climatology $u_A + u_{SC}$ . (e) Hovmoller of sea surface temperature anomalies $u_A$ . (f) Hovmoller of sea surface temperature anomalies and climatology $u_A + u_{SC}$ . (g) Hovmoller of thermocline depth anomalies $u_A$ . (h) Homvoller of thermocline depth anomalies and climatology $u_A + u_{SC}$ .	54
991 992 993	Fig. 3.	Linear trends in time of observed (a) zonal winds $u_{OBS}$ , (b) sea surface temperature $T_{OBS}$ and (c) thermocline depth $H_{OBS}$ . The trends are obtained from a polynomial curve fit of the form $u_{OBS}(x,t) = p_0(x) + p_1(x)t + o(1)$ , where $x$ is longitude, $t$ is time and $t$ 0, $t$ 1 are coefficients.	55
994 995 996 997 998	Fig. 4.	Probability density functions (PDFs) of observations. Panel (a)-(c): SST interannual anomalies $T_A$ averaged over the Nino 4, Nino 3.4 and Nino 3 regions. Panel (d)-(f): Zonal winds interannual anomalies $u_A$ averaged over the western Pacific (140E-180), the central Pacific (180-140W), and the eastern Pacific (140W-100W). Panel (g)-(i): Thermocline depth interannual anomalies $H_A$ averaged over the same regions as zonal winds. The variance (v), skewness (s) and kurtosis (k) are listed below each panel.	56
000	Fig. 5.	Same as Figure 4 but for the model surrogates	57
001 002 003	Fig. 6.	Panel (a): autocorrelation function of the total wind bursts $a_{all}$ . Panel (b): autocorrelation function of the interannual wind burst anomalies $a_A$ . Panel (c): Power spectrum of the SST averaged over the eastern half of the Pacific.	58
004 005 006	Fig. 7.	ENSO long-term memory of observations. Lagged correlations of the Nino 3.4 SST index with (a) zonal winds anomalies averaged in western Pacific $u_A^W$ , (b) zonal winds anomalies $u_A$ , (c) sea surface temperature anomalies $T_A$ , and (d) thermocline depth anomalies $H_A$	59
007 008 009 010 011	Fig. 8.	ENSO long-term memory of the coupled model. Lagged correlations between the Nino 3.4 index and (a) zonal wind anomalies averaged in the western Pacific $u_A^w$ , (b) zonal wind anomalies $u_A$ , (c) SST anomalies $T_A$ , (d) thermocline depth anomalies $H_A$ , (e) the total wind bursts $u_A$ and (f) the interannual wind burst anomalies $u_A$ . Except the total wind burst $u_A$ which contains both the interannual and high-frequency components, all the other variables including the Nino 3.4 index contain only the interannual anomalies	60
013 014 015 016 017	Fig. 9.	Same as Figure 8 but conditioned on the EP (traditional) El Niño, La Niña and CP El Niño phases. respectively. Panel (e) shows the lagged correlation between SST index and the flux divergence $\partial_x(UT)$ interannual anomalies. The Nino 3 index is utilized for computing the lagged correlations with traditional El Niño and La Niña while Nino 4 index is adopted for the CP El Niño. Note that since Nino 3 is negative at La Niña phases, a negative correlation between Nino 3 and $a_A$ corresponds to positive (westerly) wind bursts	61
019 020 021	Fig. 10.	Deterministic advection modes from the model. Panel (a): Three dynamical regimes as functions of the nonlinear advection $\mu$ and the easterly mean trade wind anomaly $\hat{a}_p$ . Panel (b)-(d): Different fields (atmosphere wind including the mean trade wind anomaly $u + \hat{u}_p$ ,	

1022 1023 1024		ocean zonal current $U$ , thermocline depth $H$ , SST $T$ , ocean Kelvin waves and ocean Rossby waves) corresponding to the three dynamical regimes, where the parameter values are marked by red dots in (a).	62
1025 1026 1027 1028 1029	Fig. 11.	Panel (a)-(d): Distribution of the waiting time $\tau_{E\to C}$ between a CP event and its previous traditional El Niño event with four different threshold values of counting the traditional El Niño before each CP event. Panel (e)-(f): Examples of CP El Niño following traditional one with two different forms. Here, each blacking bar indicates the waiting periods between one CP El Niño event and its previous traditional El Niño	 63
1030 1031 1032 1033 1034 1035 1036	Fig. 12.	Case study (I) and (II). (I) shows one moderate traditional El Niño and one super El Niño followed by a La Niña. (II) shows a series of CP El Niño followed directly by a super El Niño and then a La Niña. Different panels show (a) atmosphere wind including the mean trade wind anomaly $u+\hat{u}_p$ , (b) thermocline depth $H$ , (c) SST $T$ , (d) ocean Kelvin waves, and (e) ocean Rossby waves. All these fields are the direct model output and contain both the interannual variability and the high frequency component. Panel (f) shows the time series of the wind activity at the peak $x^*$ of the zonal profile (see Panel (b) of Figure 1) and its 90-day running average (brown curve). All variables are shown at equator	64
1038 1039 1040 1041	Fig. 13.	Case study (III) and (IV). (III) shows a series of CP El Niño followed directly by a moderate El Niño and then a La Niña. (IV) shows a series of CP El Niño followed by a few months quiescence ( $t = 416.5$ ) and then a moderate El Niño and a La Niña. The wind burst structure associated with (III) and (IV) is slightly different.	 65
1042 1043 1044 1045 1046	Fig. 14.	Case study (V) and (VI). (V) shows a moderate El Niño ( $t=478$ ) and an El Niño event being stalled by an EWB ( $t=480.8$ ) that resembles to the observational event during year 2014. (VI) shows two examples that strong wind bursts lead to no or very weak El Niño, where a clear switching between WWBs and EWBs is found in (VI.a) but the durations for both WWBs and EWBs are short while the wind bursts in (VI.b) behave like white noise.	66
1047 1048 1049 1050 1051 1052	Fig. 15.	Budget analysis of Case study (I) in Figure 12 and (IV) in Figure 13. Panel (a) and (b) show the SST $T$ and ocean zonal current $U$ . Panel (c) shows the SST tendency $dT/dt$ , which is the summation of the flux divergence $-\mu \partial_x (UT)$ (Panel (d)) and the combined effect of the damping $-c_1 \zeta E_q$ and the thermocline feedback $c_1 \eta H$ (Panel (e)). The budget components of the damping $-c_1 \zeta E_q$ and the thermocline feedback $c_1 \eta H$ are shown in Panel (f) and (g), respectively.	 67
1053 1054 1055 1056	Fig. 16.	Case study (SI): model without zonal nonlinear advection ( $\mu=0$ ) in the SST equation. Without the zonal nonlinear advection the anomalous warm SST ( $t=268-269$ and $t=278-281$ ) corresponding to State 1 shifts eastward and occurs in the traditional El Niño regions. 68	
1057 1058 1059 1060	Fig. 17.	Case study (SII): model with zero reflection coefficient in the eastern Pacific boundary $r_E=0$ . Without the reflection in the eastern Pacific boundary, the traditional El Niño is mainly dominated by Kelvin waves and the duration of these traditional El Niño, including the super El Niño, is much shorter than the realistic ones	69

### (a) Zonal profile of thermocline feedback $\eta(x)$



# (b) Zonal profile of wind burst structure $s_p(x)$



## (c) Strengthening of the trade wind anomaly at the surface

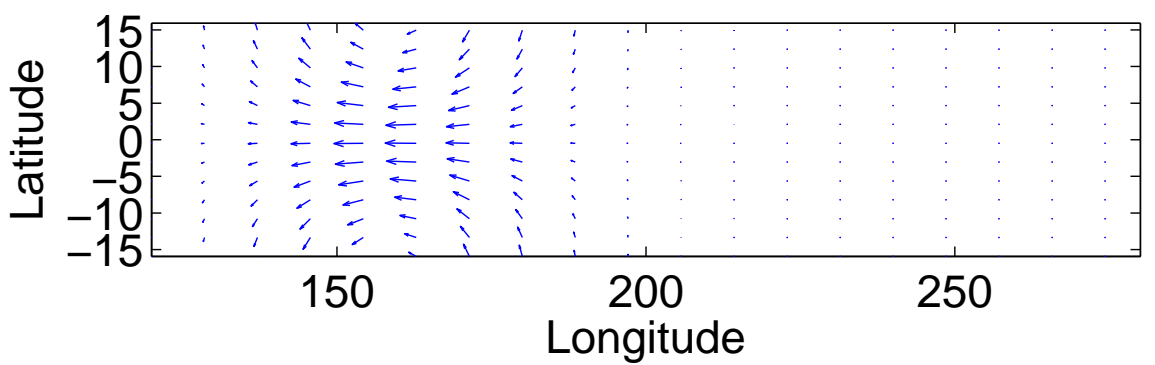


FIG. 1. (a) Zonal profile of thermocline feedback  $\eta(x)$ . (b) Zonal profile of wind burst structure  $s_p(x)$  in the western Pacific. (c) Surface wind response directly to the mean easterly trade wind anomaly  $\hat{a}_p$ , i.e.  $\hat{a}_p \cdot s_p(x) \cdot \phi_0(y)$ .

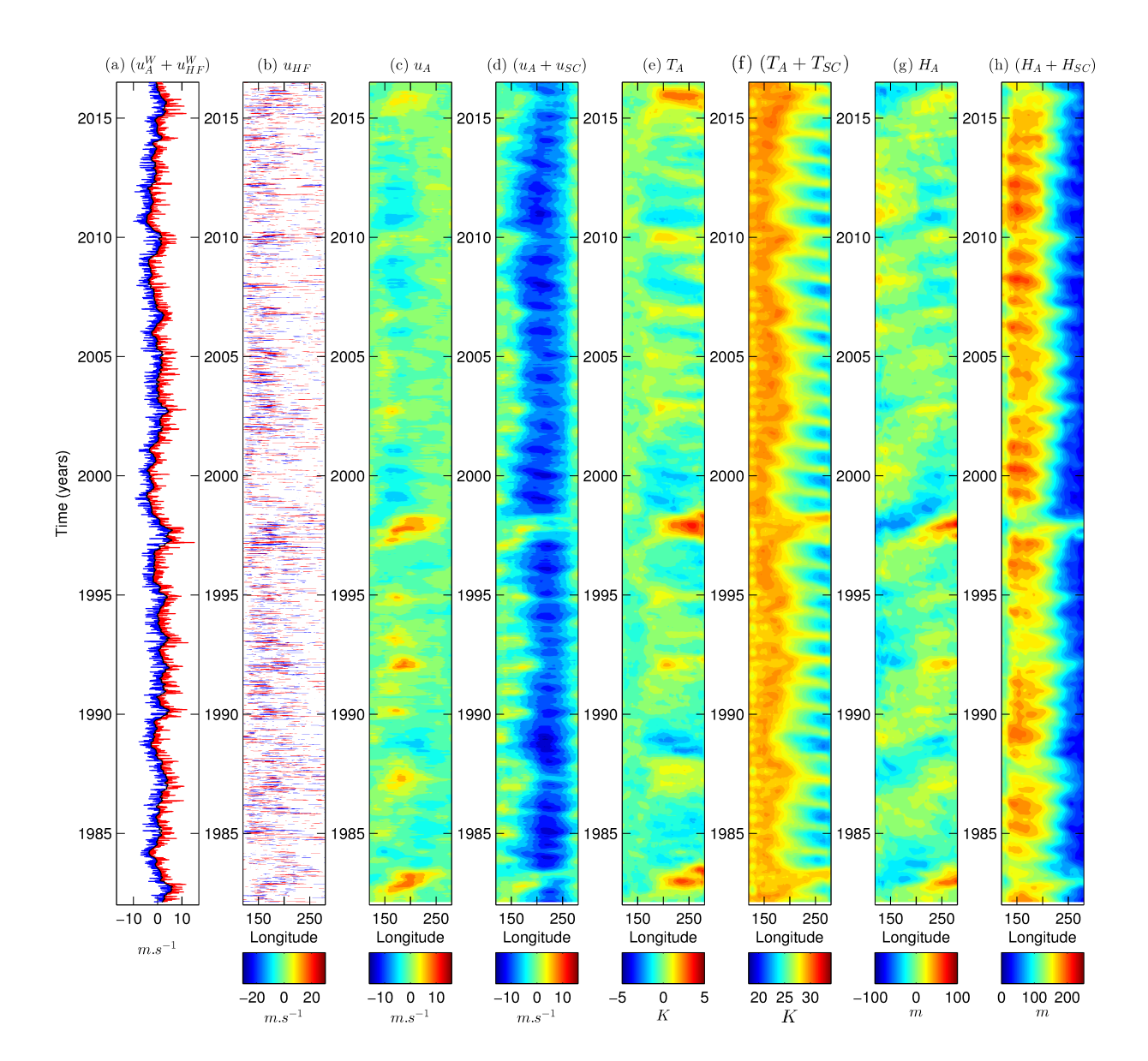


FIG. 2. Observed ENSO variability. (a) Zonal winds averaged over the western Pacific (140E-180), with a superposition of interannual  $u_A^W$  (black) and intraseasonal  $u_{HF}^W$  (blue for  $u_{HF}^W < 0$ , red for  $u_{HF}^W > 0$ ) anomalies. (b) Hovmoller of strong intraseasonal zonal winds  $u_{HF}$  (blue for  $u_{HF} \le -5 \text{ m.s}^{-1}$ , red for  $u_{HF} \ge 5 \text{ m.s}^{-1}$ ). (c) Hovmoller of zonal winds anomalies  $u_A$ . (d) Hovmoller of zonal winds anomalies and climatology  $u_A + u_{SC}$ . (e) Hovmoller of sea surface temperature anomalies  $u_A$ . (f) Hovmoller of sea surface temperature anomalies and climatology  $u_A + u_{SC}$ . (g) Hovmoller of thermocline depth anomalies  $u_A$ . (h) Homvoller of thermocline depth anomalies and climatology  $u_A + u_{SC}$ .

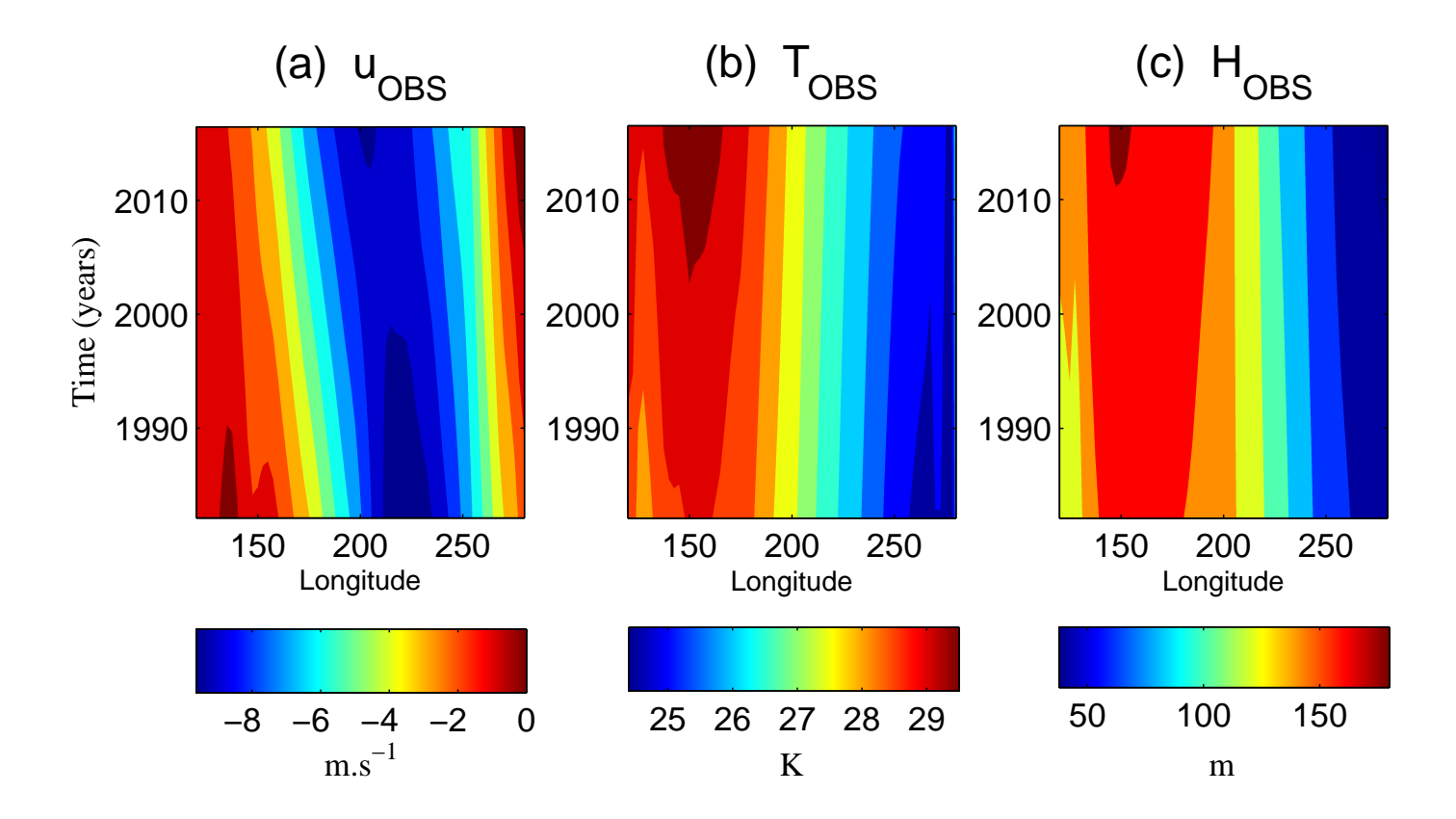


FIG. 3. Linear trends in time of observed (a) zonal winds  $u_{OBS}$ , (b) sea surface temperature  $T_{OBS}$  and (c) thermocline depth  $H_{OBS}$ . The trends are obtained from a polynomial curve fit of the form  $u_{OBS}(x,t) = p_0(x) + p_1(x)t + o(1)$ , where x is longitude, t is time and  $p_0$ ,  $p_1$  are coefficients.

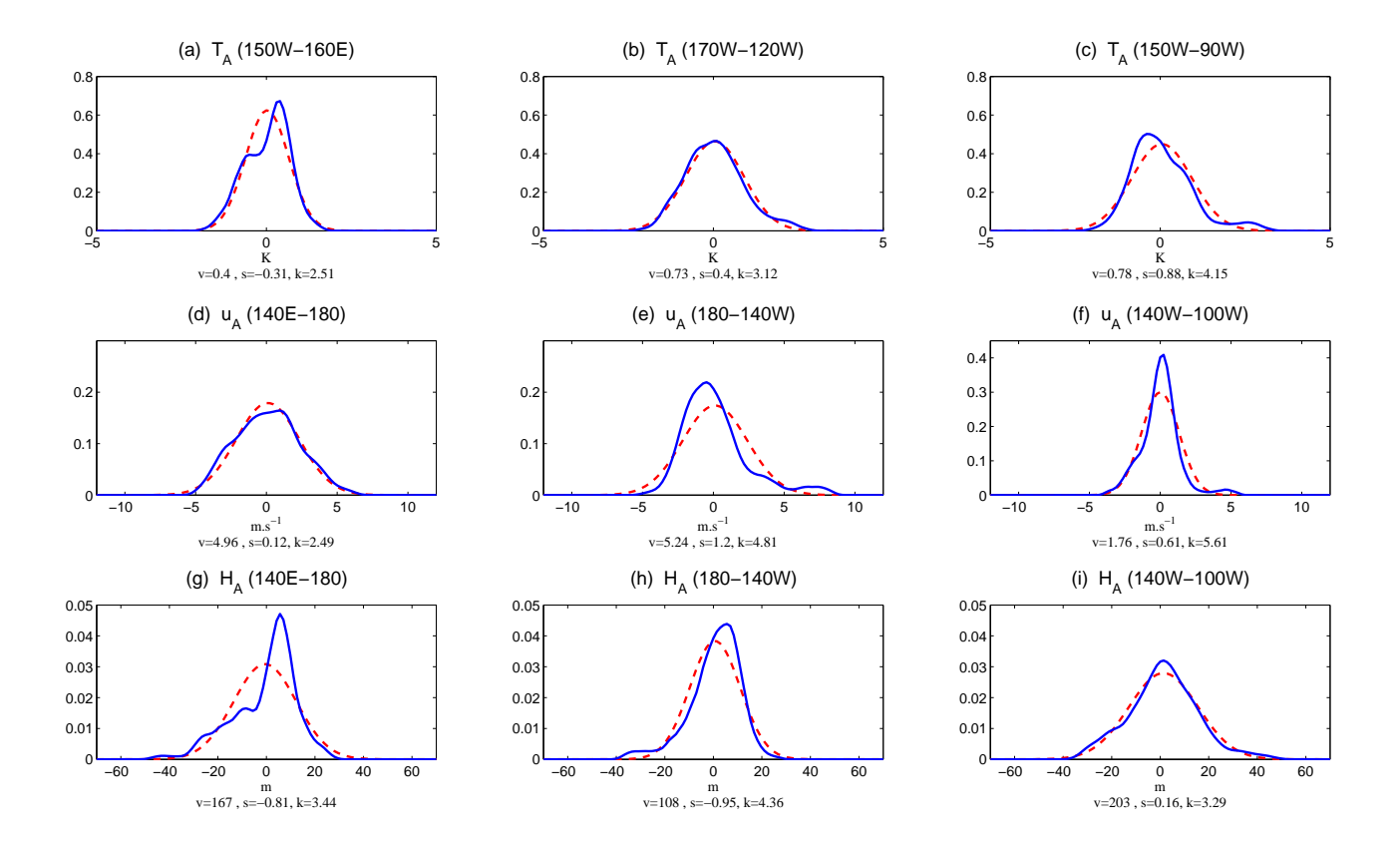


FIG. 4. Probability density functions (PDFs) of observations. Panel (a)-(c): SST interannual anomalies  $T_A$  averaged over the Nino 4, Nino 3.4 and Nino 3 regions. Panel (d)-(f): Zonal winds interannual anomalies  $u_A$  averaged over the western Pacific (140E-180), the central Pacific (180-140W), and the eastern Pacific (140W-100W). Panel (g)-(i): Thermocline depth interannual anomalies  $H_A$  averaged over the same regions as zonal winds. The variance (v), skewness (s) and kurtosis (k) are listed below each panel.

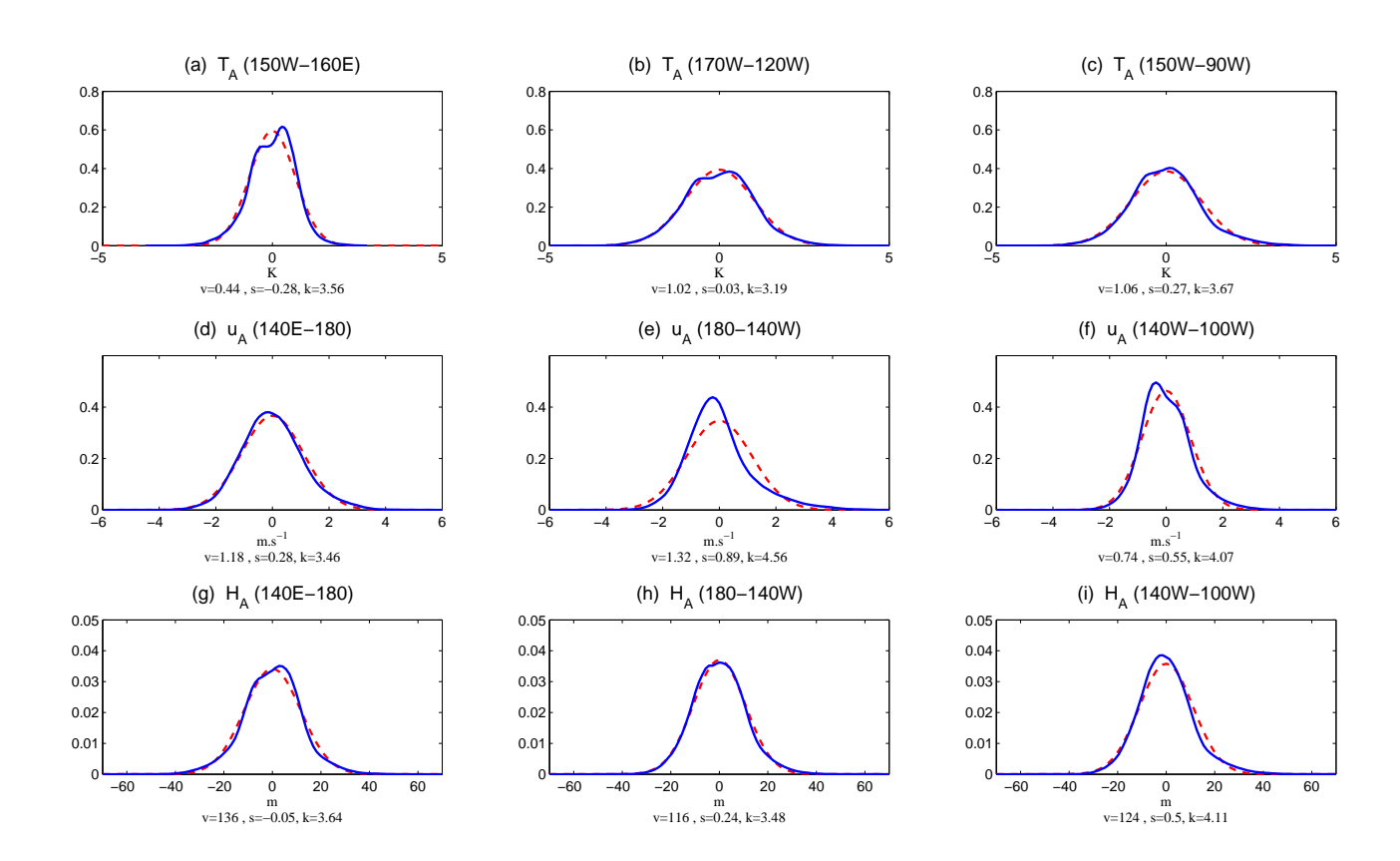


FIG. 5. Same as Figure 4 but for the model surrogates.

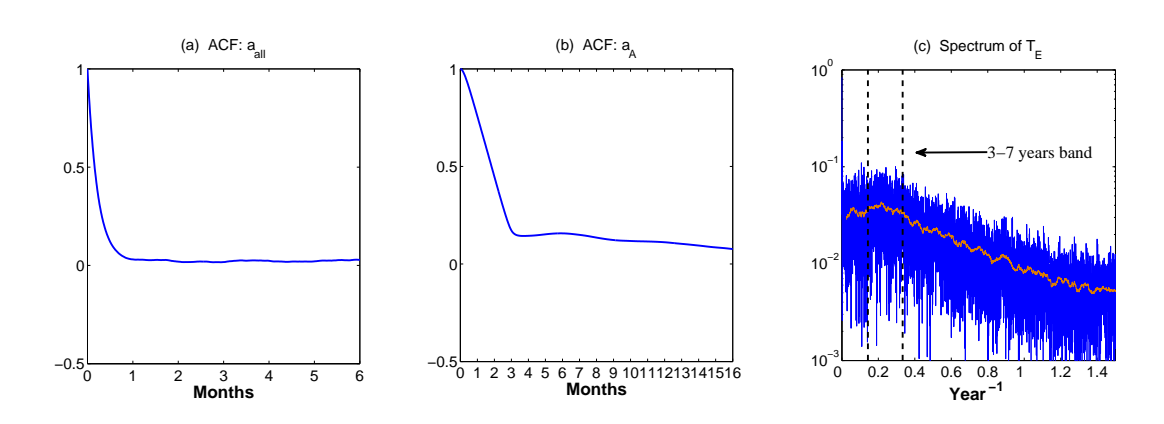


FIG. 6. Panel (a): autocorrelation function of the total wind bursts  $a_{all}$ . Panel (b): autocorrelation function of the interannual wind burst anomalies  $a_A$ . Panel (c): Power spectrum of the SST averaged over the eastern half of the Pacific.

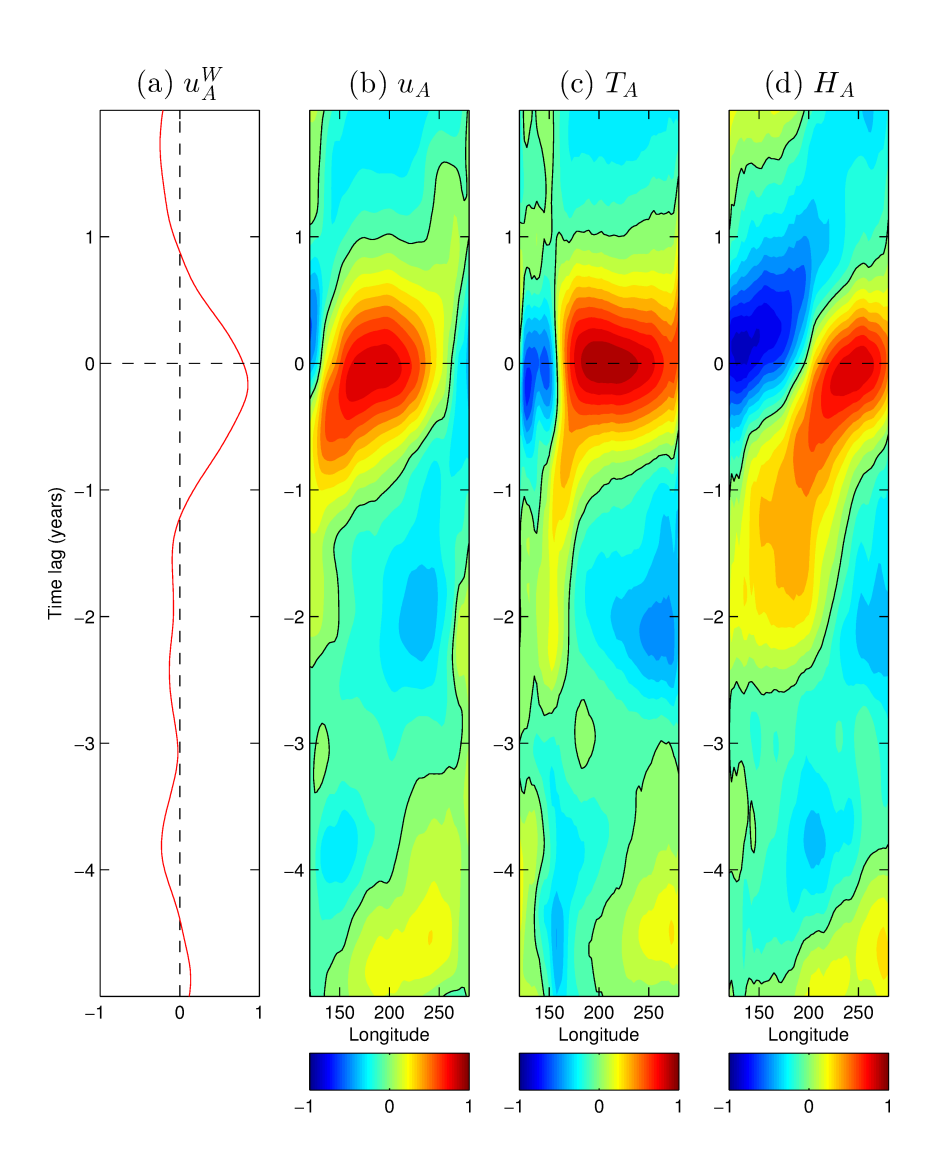


FIG. 7. ENSO long-term memory of observations. Lagged correlations of the Nino 3.4 SST index with (a) zonal winds anomalies averaged in western Pacific  $u_A^W$ , (b) zonal winds anomalies  $u_A$ , (c) sea surface temperature anomalies  $T_A$ , and (d) thermocline depth anomalies  $H_A$ .

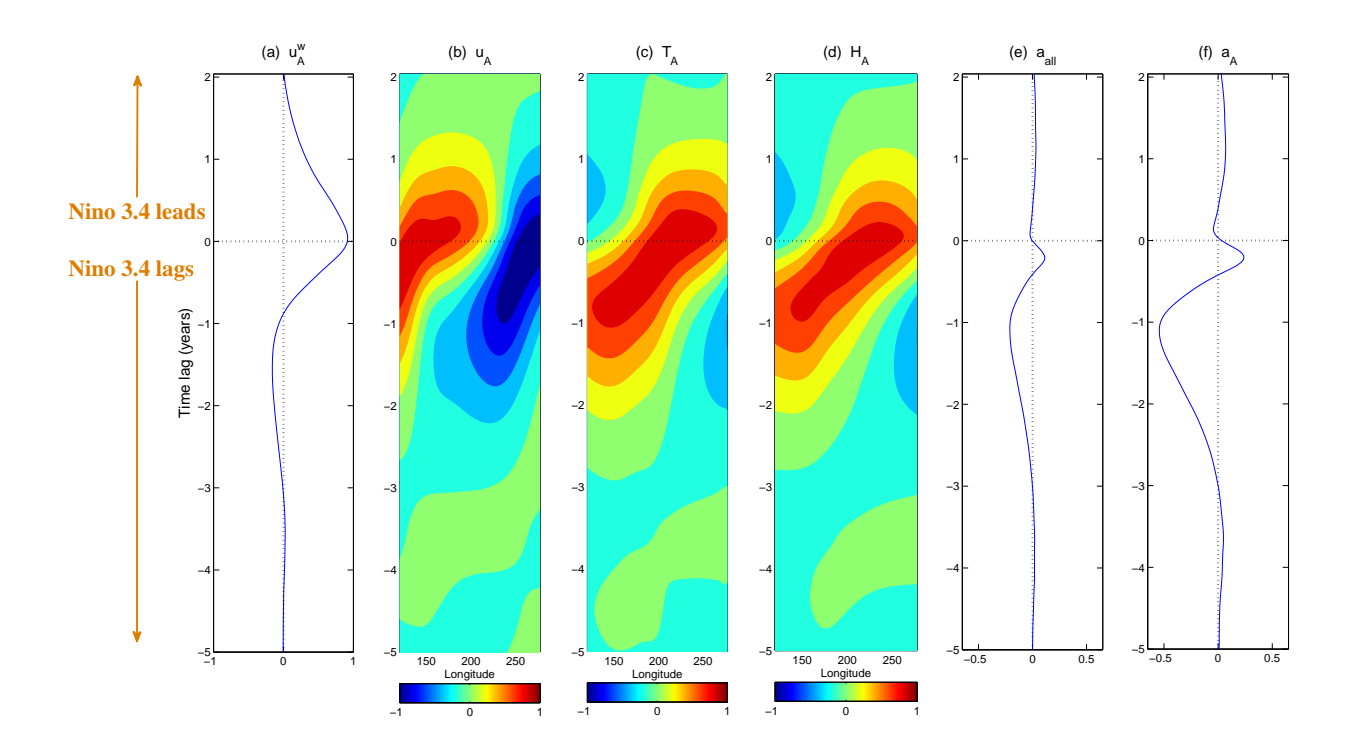


FIG. 8. ENSO long-term memory of the coupled model. Lagged correlations between the Nino 3.4 index and (a) zonal wind anomalies averaged in the western Pacific  $u_A^w$ , (b) zonal wind anomalies  $u_A$ , (c) SST anomalies  $T_A$ , (d) thermocline depth anomalies  $H_A$ , (e) the total wind bursts  $a_{all}$  and (f) the interannual wind burst anomalies  $a_A$ . Except the total wind burst  $a_{all}$  which contains both the interannual and high-frequency components, all the other variables including the Nino 3.4 index contain only the interannual anomalies.

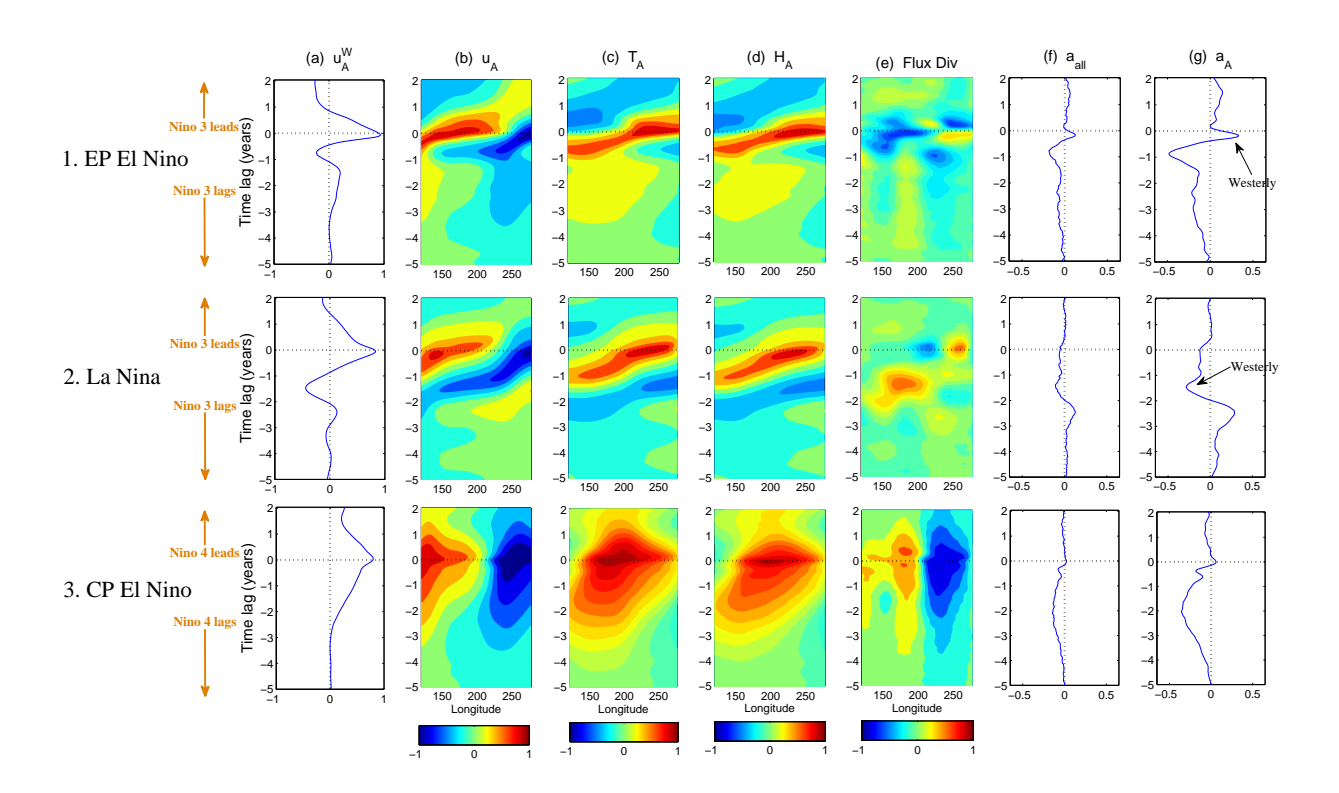


FIG. 9. Same as Figure 8 but conditioned on the EP (traditional) El Niño, La Niña and CP El Niño phases. respectively. Panel (e) shows the lagged correlation between SST index and the flux divergence  $\partial_x(UT)$  interannual anomalies. The Nino 3 index is utilized for computing the lagged correlations with traditional El Niño and La Niña while Nino 4 index is adopted for the CP El Niño. Note that since Nino 3 is negative at La Niña phases, a negative correlation between Nino 3 and  $a_A$  corresponds to positive (westerly) wind bursts.

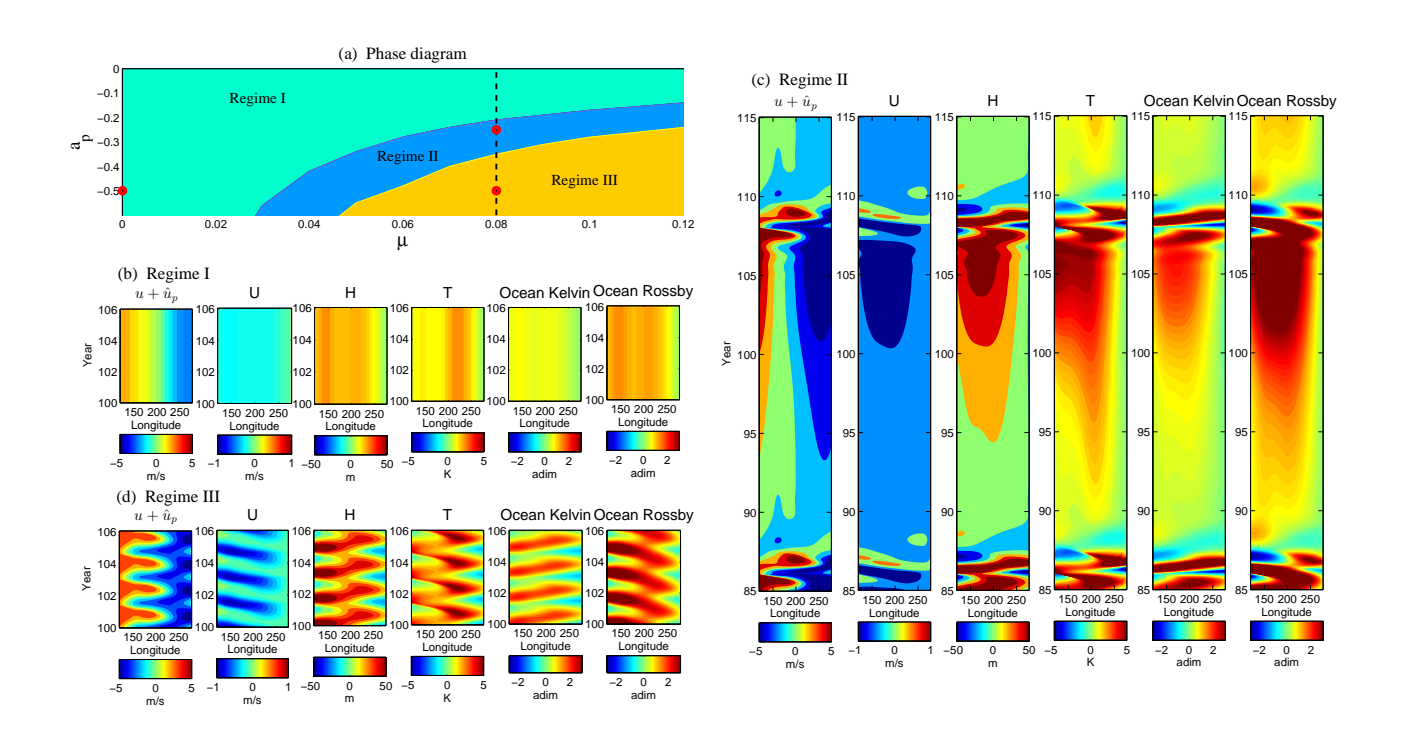


FIG. 10. Deterministic advection modes from the model. Panel (a): Three dynamical regimes as functions of the nonlinear advection  $\mu$  and the easterly mean trade wind anomaly  $\hat{a}_p$ . Panel (b)-(d): Different fields (atmosphere wind including the mean trade wind anomaly  $u + \hat{u}_p$ , ocean zonal current U, thermocline depth H, SST T, ocean Kelvin waves and ocean Rossby waves) corresponding to the three dynamical regimes, where the parameter values are marked by red dots in (a).

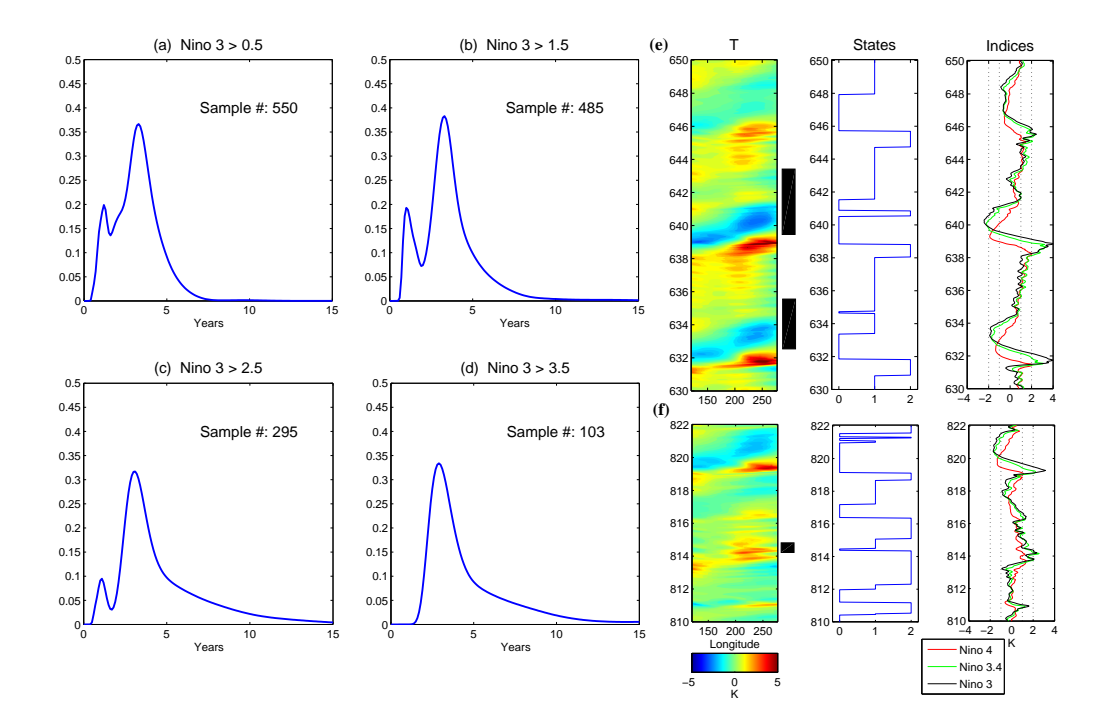


FIG. 11. Panel (a)-(d): Distribution of the waiting time  $\tau_{E\to C}$  between a CP event and its previous traditional El Niño event with four different threshold values of counting the traditional El Niño before each CP event.

Panel (e)-(f): Examples of CP El Niño following traditional one with two different forms. Here, each blacking bar indicates the waiting periods between one CP El Niño event and its previous traditional El Niño.

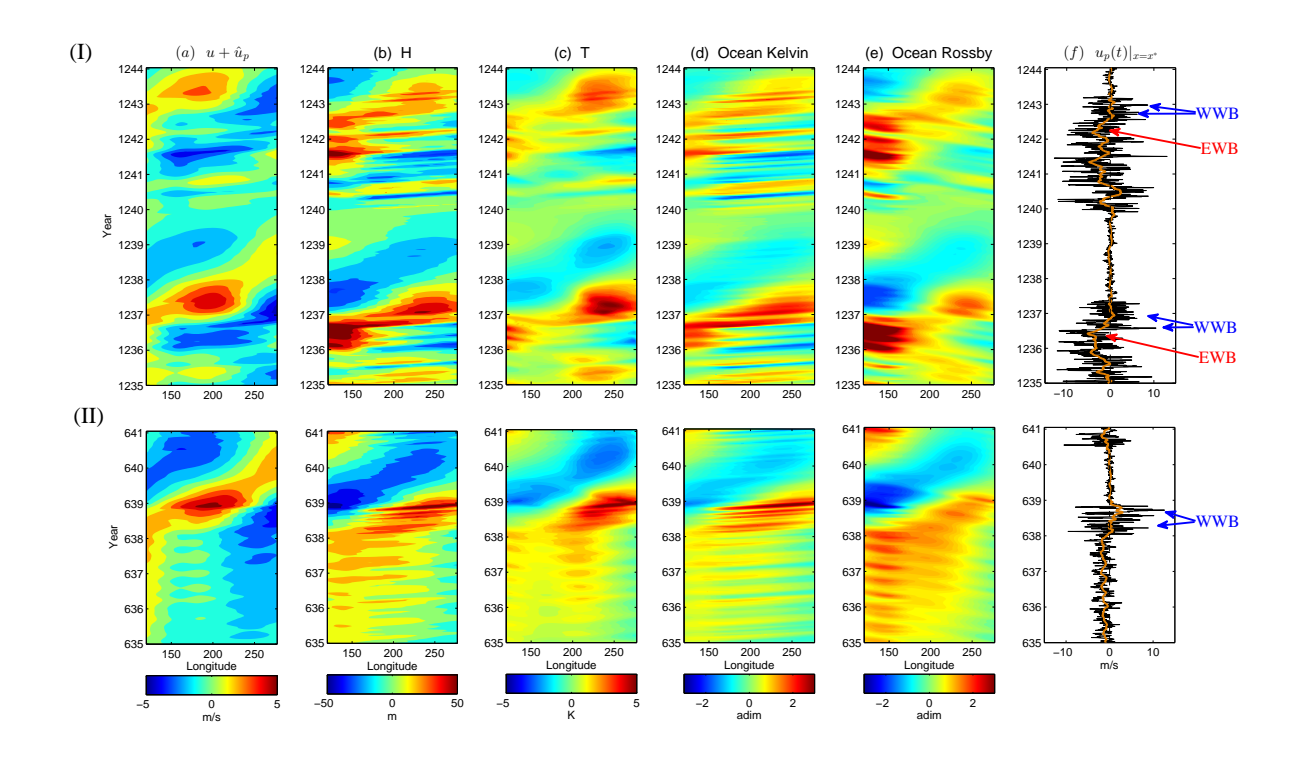


FIG. 12. Case study (I) and (II). (I) shows one moderate traditional El Niño and one super El Niño followed by a La Niña. (II) shows a series of CP El Niño followed directly by a super El Niño and then a La Niña. Different panels show (a) atmosphere wind including the mean trade wind anomaly  $u + \hat{u}_p$ , (b) thermocline depth H, (c) SST T, (d) ocean Kelvin waves, and (e) ocean Rossby waves. All these fields are the direct model output and contain both the interannual variability and the high frequency component. Panel (f) shows the time series of the wind activity at the peak  $x^*$  of the zonal profile (see Panel (b) of Figure 1) and its 90-day running average (brown curve). All variables are shown at equator.

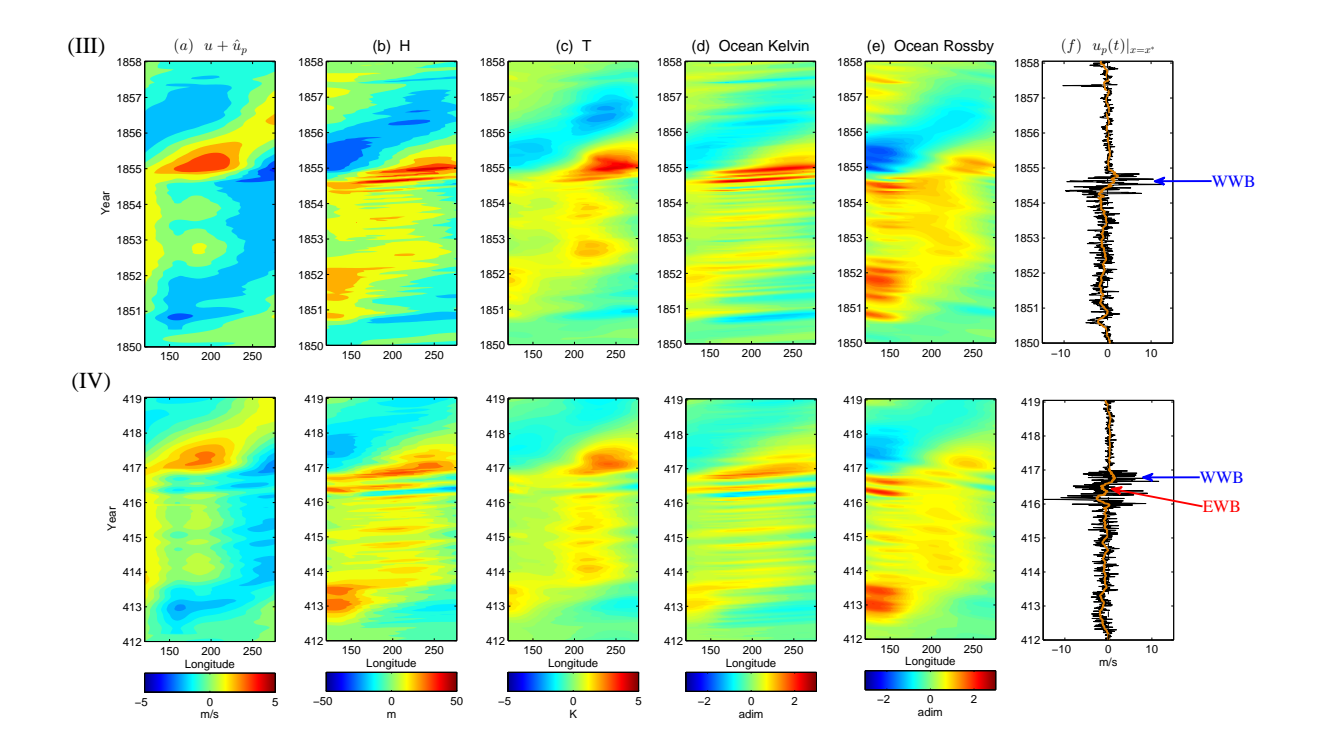


FIG. 13. Case study (III) and (IV). (III) shows a series of CP El Niño followed directly by a moderate El Niño and then a La Niña. (IV) shows a series of CP El Niño followed by a few months quiescence (t = 416.5) and then a moderate El Niño and a La Niña. The wind burst structure associated with (III) and (IV) is slightly different.

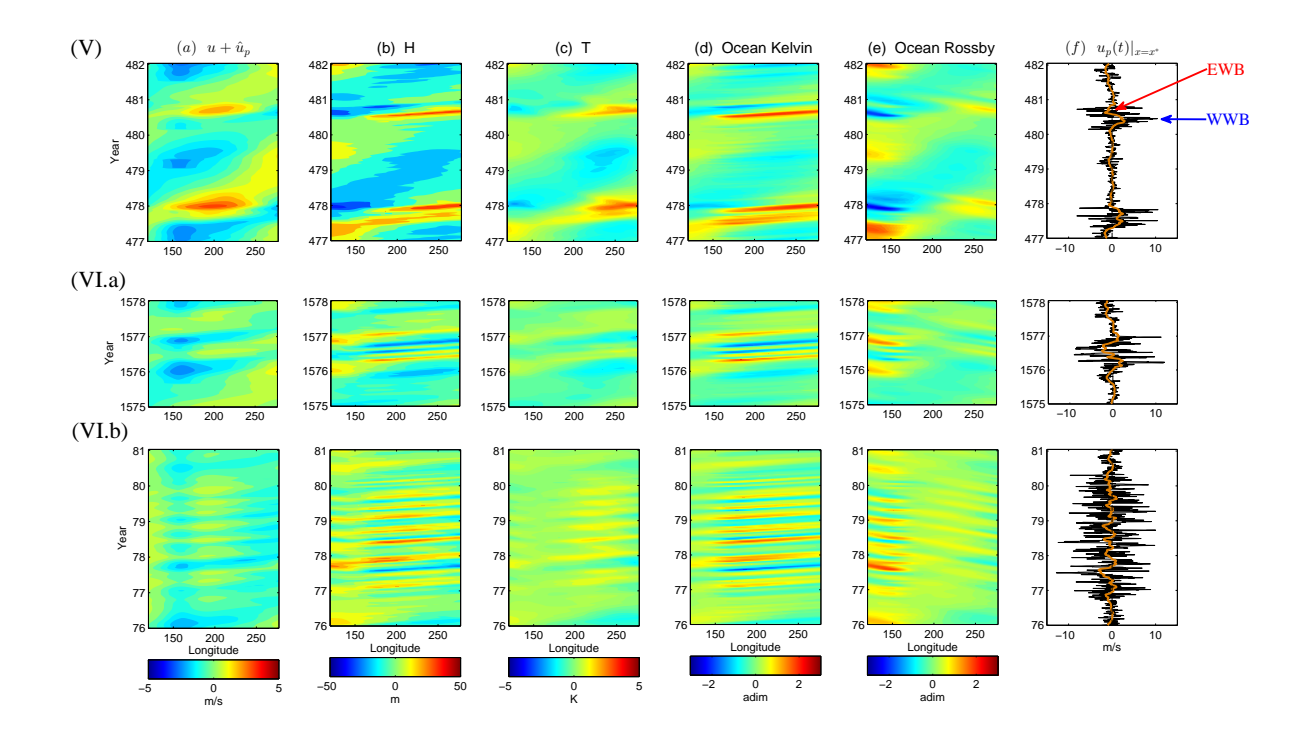


FIG. 14. Case study (V) and (VI). (V) shows a moderate El Niño (t = 478) and an El Niño event being stalled by an EWB (t = 480.8) that resembles to the observational event during year 2014. (VI) shows two examples that strong wind bursts lead to no or very weak El Niño, where a clear switching between WWBs and EWBs is found in (VI.a) but the durations for both WWBs and EWBs are short while the wind bursts in (VI.b) behave like white noise.

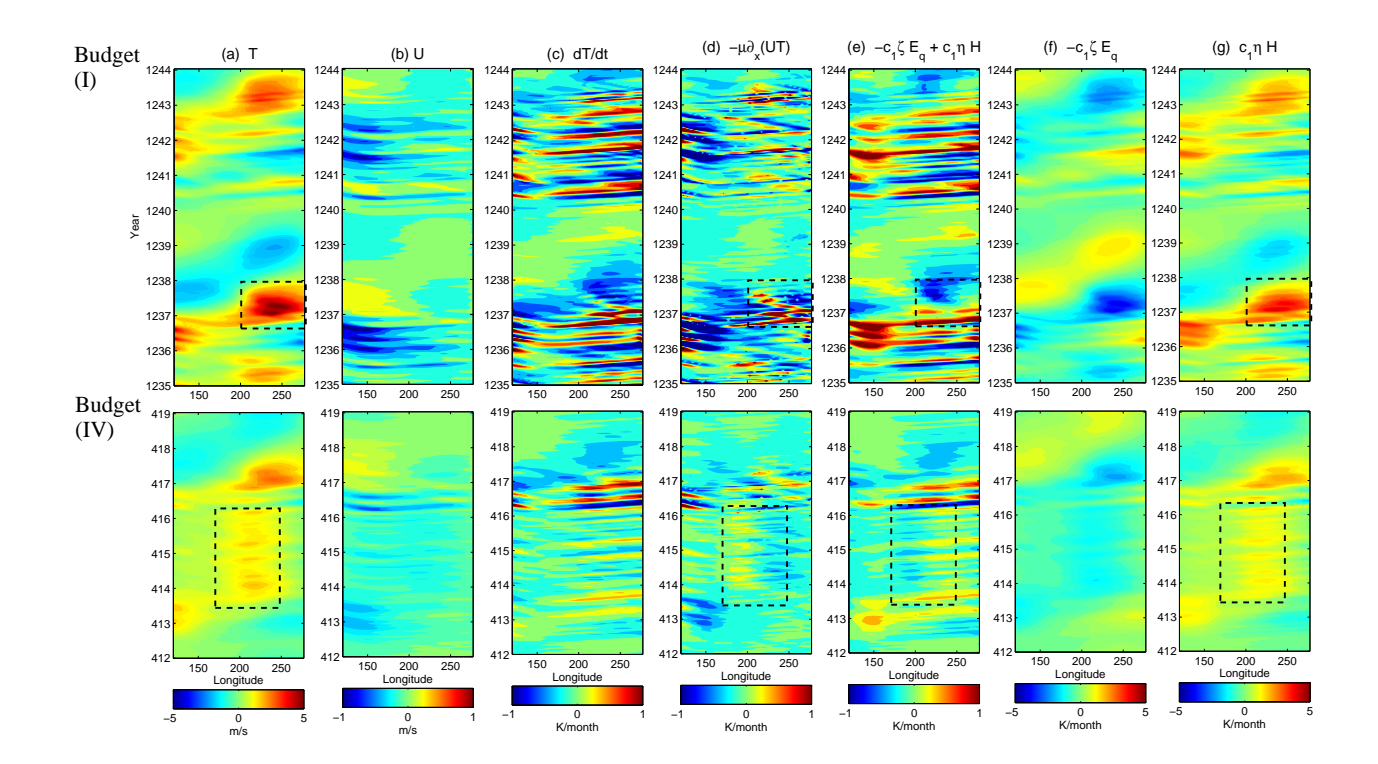


FIG. 15. Budget analysis of Case study (I) in Figure 12 and (IV) in Figure 13. Panel (a) and (b) show the SST T and ocean zonal current U. Panel (c) shows the SST tendency dT/dt, which is the summation of the flux divergence  $-\mu \partial_x (UT)$  (Panel (d)) and the combined effect of the damping  $-c_1 \zeta E_q$  and the thermocline feedback  $c_1 \eta H$  (Panel (e)). The budget components of the damping  $-c_1 \zeta E_q$  and the thermocline feedback  $c_1 \eta H$  are shown in Panel (f) and (g), respectively.

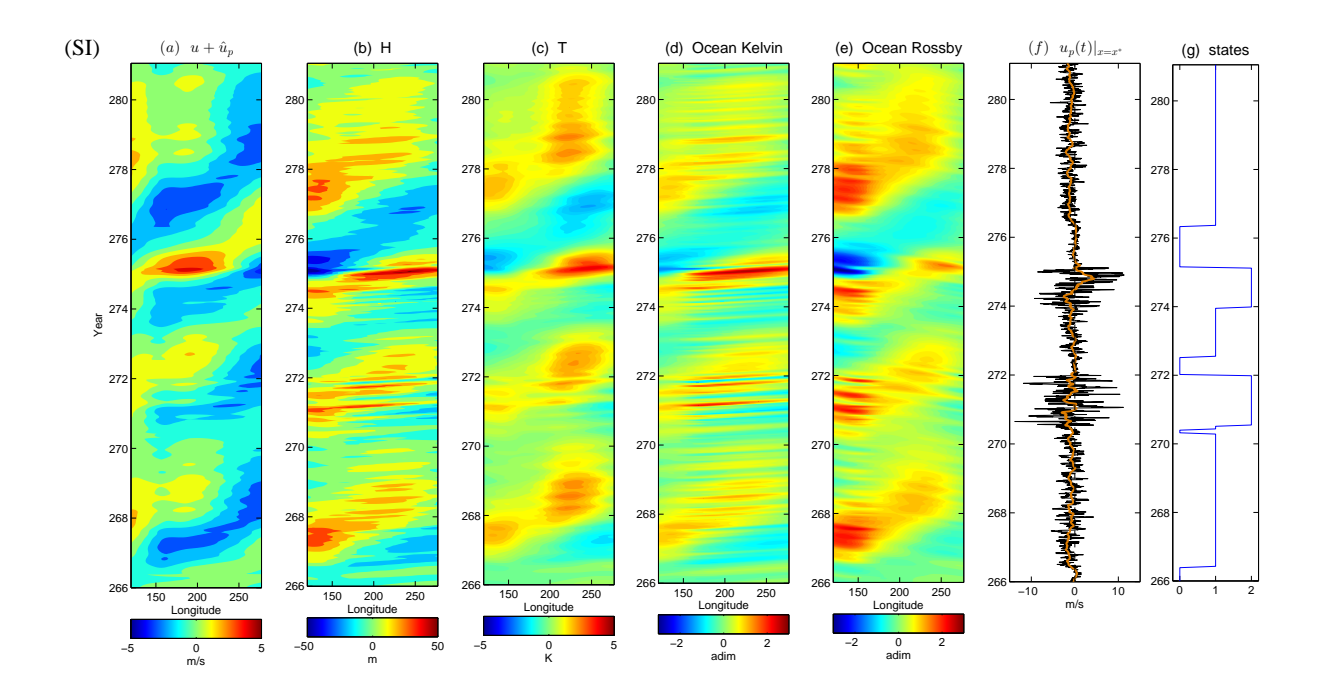


FIG. 16. Case study (SI): model without zonal nonlinear advection ( $\mu = 0$ ) in the SST equation. Without the zonal nonlinear advection the anomalous warm SST (t = 268-269 and t = 278-281) corresponding to State 1 shifts eastward and occurs in the traditional El Niño regions.

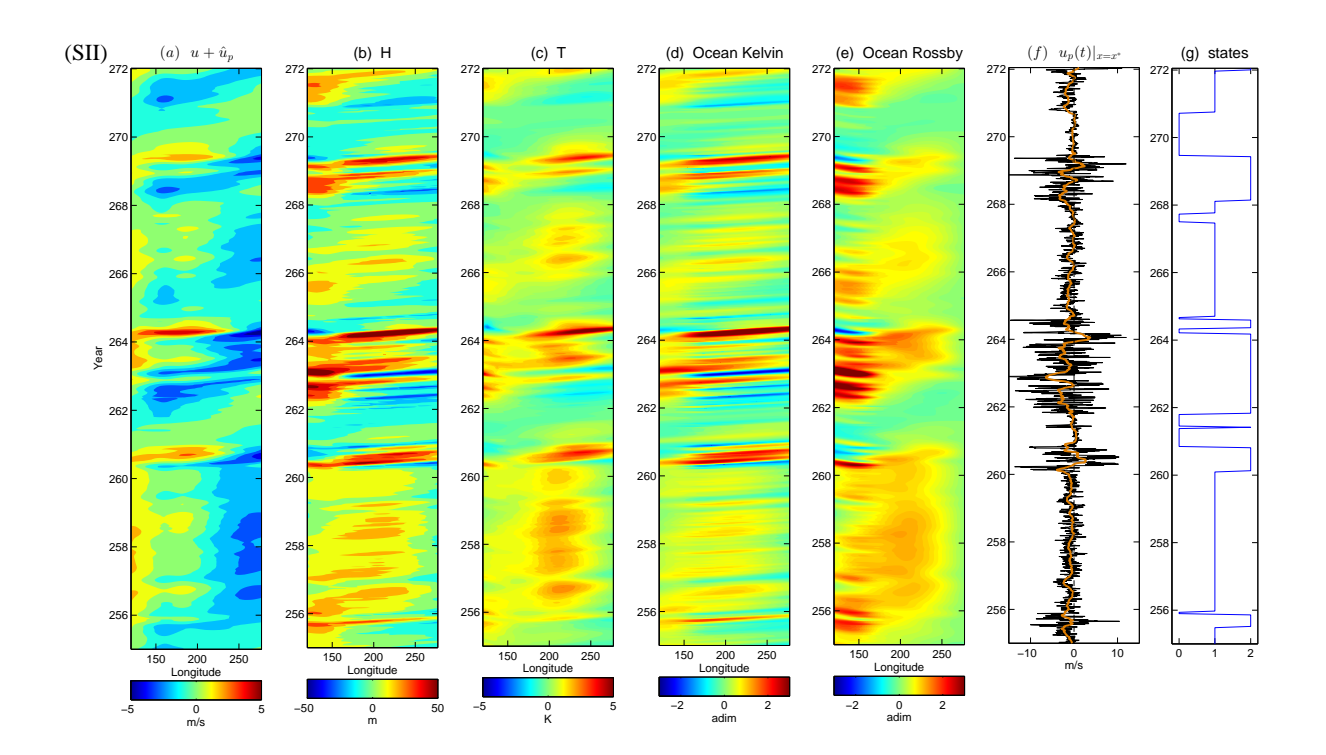


FIG. 17. Case study (SII): model with zero reflection coefficient in the eastern Pacific boundary  $r_E = 0$ .
Without the reflection in the eastern Pacific boundary, the traditional El Niño is mainly dominated by Kelvin waves and the duration of these traditional El Niño, including the super El Niño, is much shorter than the realistic ones.